




ARTICLE

Macrophage galactose lectin is critical for Kupffer cells to clear aged platelets

Carsten Deppermann^{1,2,3} , Rachel M. Kratochvil^{1,2} , Moritz Peiseler^{1,2}, Bruna A. David^{1,2}, Joel Zindel^{1,2}, Fernanda Vargas E Silva Castanheira^{1,2}, Fardau van der Wal^{1,2}, Agostina Carestia^{2,4}, Craig N. Jenne^{2,4}, Jamey D. Marth⁵, and Paul Kubes^{1,2} 

Every day, megakaryocytes produce billions of platelets that circulate for several days and eventually are cleared by the liver. The exact removal mechanism, however, remains unclear. Loss of sialic acid residues is thought to feature in the aging and clearance of platelets. Using state-of-the-art spinning disk intravital microscopy to delineate the different compartments and cells of the mouse liver, we observed rapid accumulation of desialylated platelets predominantly on Kupffer cells, with only a few on endothelial cells and none on hepatocytes. Kupffer cell depletion prevented the removal of aged platelets from circulation. Ashwell-Morell receptor (AMR) deficiency alone had little effect on platelet uptake. Macrophage galactose lectin (MGL) together with AMR mediated clearance of desialylated or cold-stored platelets by Kupffer cells. Effective clearance is critical, as mice with an aged platelet population displayed a bleeding phenotype. Our data provide evidence that the MGL of Kupffer cells plays a significant role in the removal of desialylated platelets through a collaboration with the AMR, thereby maintaining a healthy and functional platelet compartment.

Introduction

Platelets are small, anucleated cells that patrol the vasculature to maintain hemostasis. The human body produces 100 billion platelets every day from bone marrow megakaryocytes that then circulate in the bloodstream for several days (Quach et al., 2018). Platelet formation (thrombopoiesis) during both homeostatic and emergency conditions has been investigated in great detail (Junt et al., 2007; Bender et al., 2014; Nishimura et al., 2015), and decreased production of platelets, improper function of their various adhesion molecules, or over-exuberant clearance leads to untoward bleeding and, in severe cases, death. By contrast, the cell types and mechanism(s) by which aged platelets are removed from circulation remain poorly understood. Aster and colleagues showed in the late 1960s that transfused platelets accumulated in the liver of healthy volunteers (Aster and Jandl, 1964; Aster, 1969); however, the mechanism by which they were trapped remained incompletely understood. In the 1970s, it was demonstrated that there were large differences in the recovery of transfused platelets depending on their storage conditions. Platelets stored at 4°C were rapidly cleared from circulation after transfusion, whereas room temperature-stored platelets showed significantly better recovery rates (Becker et al., 1973).

Storage at room temperature, however, carries the inherent risk of bacterial contamination and also causes a decline in platelet functionality known as the platelet storage lesion, which is characterized by platelet degranulation and changes in morphology (Devine and Serrano, 2010). In 2003, Hoffmeister and colleagues found that cold-stored platelets cluster the von Willebrand factor (vWF) receptor glycoprotein Ib (GPIb) on their surface, which upon platelet transfusion led to their recognition by liver macrophages through $\alpha_M\beta_2$ integrin (Hoffmeister et al., 2003a). $\alpha_M\beta_2$ recognizes GPIb on cooled platelets through a lectin-mediated interaction with exposed β -N-acetylglucosamine residues on N-linked oligosaccharides (Hoffmeister et al., 2003b). The group also proposed that the interaction between GPIb and $\alpha_M\beta_2$ could be blocked by galactosylation of exposed β -N-acetylglucosamine residues. However, in a phase I clinical trial, galactosylation of human platelets did not prevent accelerated platelet clearance observed after cold storage (Wandall et al., 2008).

The Ashwell-Morell receptor (AMR) is the prototype asialoglycoprotein receptor and the major lectin expressed on hepatocytes. AMR has the capacity to rapidly clear glycoproteins

¹Department of Physiology and Pharmacology, University of Calgary, Calgary, Alberta, Canada; ²Calvin, Phoebe and Joan Snyder Institute for Chronic Diseases, University of Calgary, Calgary, Alberta, Canada; ³Institute of Clinical Chemistry and Laboratory Medicine, University Medical Center Hamburg-Eppendorf, Hamburg, Germany; ⁴Department of Microbiology, Immunology and Infectious Diseases, University of Calgary, Calgary, Alberta, Canada; ⁵Center for Nanomedicine, SBP Medical Discovery Institute, and Department of Molecular, Cellular, and Developmental Biology, University of California, Santa Barbara, Santa Barbara, CA.

Correspondence to Paul Kubes: pkubes@ucalgary.ca.

© 2020 Crown copyright. The government of Australia, Canada, or the UK ("the Crown") owns the copyright interests of authors who are government employees. The Crown Copyright is not transferable. This article is distributed under the terms of an Attribution-Noncommercial-Share Alike-No Mirror Sites license for the first six months after the publication date (see <http://www.rupress.org/terms/>). After six months it is available under a Creative Commons License (Attribution-Noncommercial-Share Alike 4.0 International license, as described at <https://creativecommons.org/licenses/by-nc-sa/4.0/>).

from blood circulation that have exposed galactose linkages (Ashwell and Morell, 1974; Tozawa et al., 2001; Grewal, 2010; Rice et al., 2003; Yang et al., 2015). These so-called asialoglycoprotein ligands of the AMR are formed following desialylation of the nascent proteins during aging (Yang et al., 2015, 2018). *Streptococcus pneumoniae* and other respiratory pathogens express sialidases (neuraminidases) as virulence factors that desialylate vWF and platelets to induce an early moderate thrombocytopenia dependent upon the AMR (Grewal et al., 2008, 2013). Similarly, mice lacking the sialyltransferase ST3Gal-IV, which transfers sialic acid in an $\alpha 2,3$ linkage to glycans with terminal galactose residues, display thrombocytopenia due to reduced platelet protein sialylation (Sørensen et al., 2009; Ellies et al., 2002), and this defect could be corrected in part by AMR deletion (Grewal et al., 2008). While the AMR was necessary for platelet clearance in some contexts, AMR deficiency had a small or negligible effect on platelet numbers in healthy mice (Grewal et al., 2008, 2013; Grozovsky et al., 2015a).

Although the AMR modulates the rate of platelet clearance to some extent, the mechanisms involved, including the tissues and cell types, have not been fully elucidated partly due to indirect methods examining platelet clearance. For example, biotin-labeled cold-stored platelets had increased density of galactose residues, and biotin was greatly increased in hepatocytes, mediated in part by the AMR (Rumjantseva et al., 2009). These refrigerated platelets in vitro were phagocytosed avidly by a hepatocyte cell line, leading to the conclusion that hepatocytes take up and remove cold-stored platelets. However, others have shown that the upper size limit of particles that are processed by hepatocytes is 70 nm in diameter or close to 10-fold smaller than platelets (Rensen et al., 2001). This is likely due to the fact that the fenestrations in murine liver sinusoidal endothelial cells are ~ 180 nm in size (Zapotoczny et al., 2017), making it unlikely that murine platelets (500 nm in diameter) could cross the endothelium, access the space of Disse, and come in direct contact with hepatocytes (Schmitt et al., 2001). Nevertheless, it is possible that molecules released from platelets do come in contact with hepatocytes, especially since hepatocytes are implicated in controlling platelet numbers by thrombopoietin production, thereby driving platelet formation by megakaryocytes in the bone marrow (Grozovsky et al., 2015a). Platelets lose their sialic acid residues as they circulate and then are cleared by the liver, although the mechanisms of platelet turnover have remained a mystery. Aged platelets have previously been associated with reduced functionality (Peng et al., 1994), thereby underscoring the importance of understanding platelet removal from circulation.

The liver possesses the largest population of immobilized professional phagocytes called Kupffer cells, which are F4/80⁺ macrophages that reside in the vascular space firmly attached to the sinusoids (Bilzer et al., 2006). Their primary goal is to remove large particles such as bacteria, viruses, and foreign objects (beads) in an amazingly effective manner (Helmy et al., 2006; Zeng et al., 2016). As such, Kupffer cells seem to be well positioned to contribute to the removal of aged platelets from the circulation under homeostatic conditions. Recently, it was suggested that O-glycan desialylation caused transfused platelets to

roll on hepatocyte microvilli and bind to Kupffer cells, which contributed to removal of platelets (Li et al., 2017). Clearly, there is still uncertainty over the key cell in platelet removal, the molecular mechanisms that are involved, and the differences from model to model used. To date, there is essentially no data regarding how, during homeostasis, an aging platelet is removed from normal healthy mammals.

Here, we used high-resolution dual-laser spinning disk intravital microscopy (SD-IVM), which enabled us to delineate the three key players (Kupffer cells [purple], sinusoidal endothelium [blue], and the hepatocytes [autofluorescent green], Fig. 1 A) and examined the in vivo processes of naturally aged platelet clearance and the processes unfolding after platelet desialylation in vivo to mimic aging as well as certain infections where bacterial sialidase is increased. We have demonstrated using intravital imaging that under basal conditions, platelets continuously touch down and let go on Kupffer cells, and a small percentage of the platelets remained arrested on the Kupffer cells and were ingested. We do not see this type of platelet interaction in other organs. While this was fairly rare, blocking this event led to increased aged platelets in blood. Similarly, when we desialylated platelets (model of aging), we observed rapid accumulation almost exclusively on Kupffer cells but not on hepatocytes or endothelium. Moreover, removal of Kupffer cells dramatically increased the number of desialylated platelets in the circulation. Combining AMR deficiency with blocking of macrophage galactose lectin (MGL) resulted in almost completely abolished adhesion of desialylated platelets to Kupffer cells and their subsequent uptake. Interrupting this process led to the accumulation of aged platelets and increased bleeding.

Results

SD-IVM of the liver allows precise localization of platelet clearance

Using SD-IVM of the mouse liver allows us to study immunological processes in the liver in vivo with great spatiotemporal resolution. Highlighted in Fig. 1 A are a cartoon and an image of the mouse liver architecture. The Kupffer cells reside inside the sinusoids firmly attached to the endothelium (Fig. 1 A and Video 1). The fenestrated endothelium allows particles smaller than 180 nm to move into the space of Disse for direct exposure to hepatocytes. Platelets and other blood-borne cells are restricted from entering the space of Disse (Wisse et al., 1996; Wisse, 1970; Zapotoczny et al., 2017). i.v. delivery of antibodies allows us to specifically label the Kupffer cells (anti-F4/80), the endothelium (anti-CD31), and the platelets (anti-CD49b, shown later), while the hepatocytes are autofluorescent and thus require no labeling. All these cells can be specifically stained and identified in an anesthetized mouse with unperturbed liver blood flow.

To fully confirm that the imaging setup used would be able to distinguish between the vasculature and the extravascular space of Disse and hepatocytes, we imaged the spatial distribution of fluorescently labeled dextran (rapidly cleared) and albumin, which is briefly retained in vasculature and taken up by the endothelium over 24 h after i.v. administration. We observed the accumulation of dextran in hepatocytes (Fig. 1 B). By contrast,

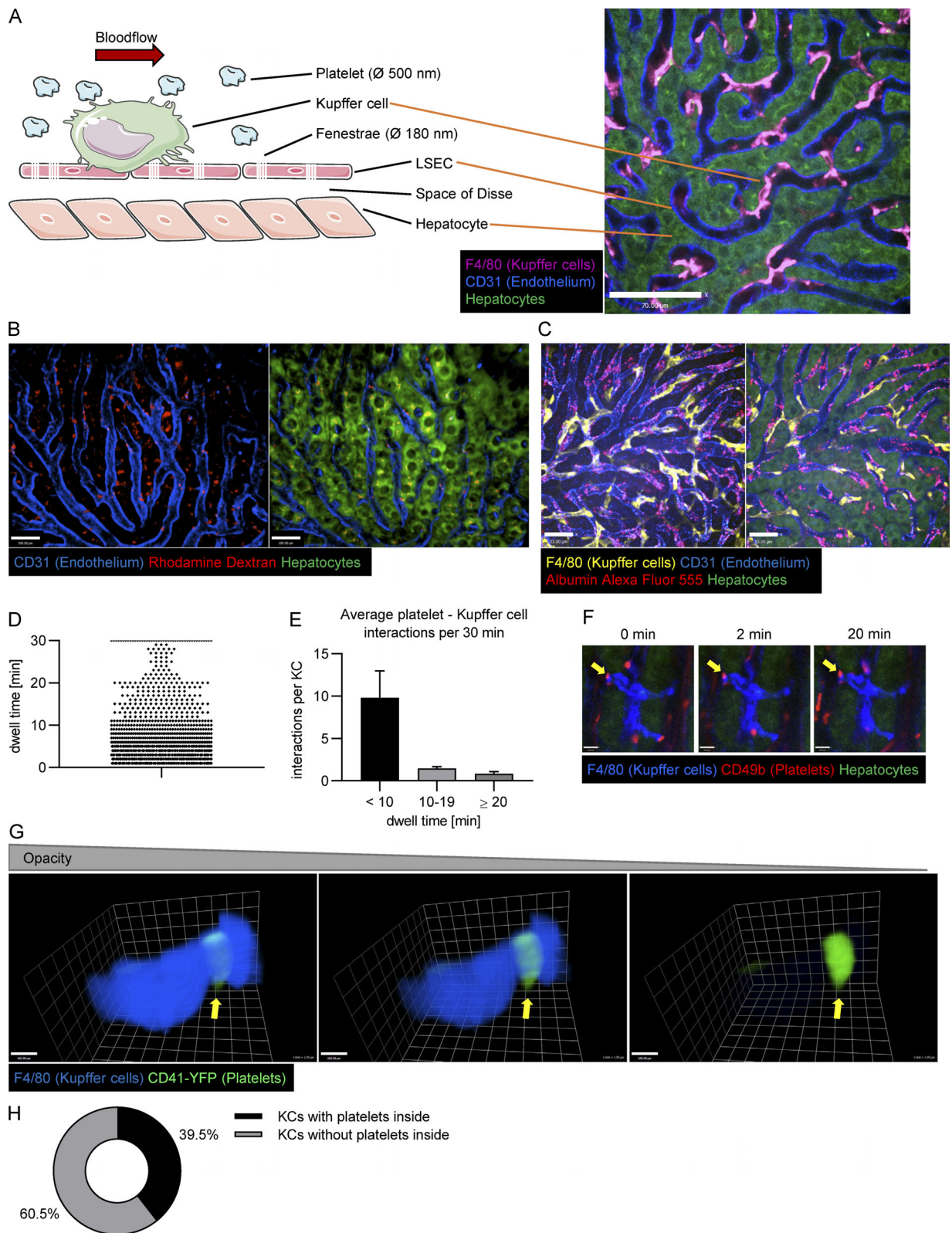


Figure 1. SD-IVM of the liver allows one to pinpoint the location of platelet clearance and to analyze platelet Kupffer cell interactions in the steady state. (A) Schematic depiction of the liver structure (left) and example image of the mouse liver (right) show that crucial components of the liver can be stained and visualized using SD-IVM. Kupffer cells and endothelial cells were stained using fluorescently labeled anti-F4/80 and anti-CD31 antibody, respectively. LSEC, liver sinusoidal endothelial cell; Ø, diameter. Scale bar is 70 µm. (B) 3D reconstruction of a 15-µm z-stack obtained using SD-IVM of the mouse liver 24 h after injecting rhodamine dextran shows colocalization of dextran staining and hepatocytes (overlay of red dextran with green hepatocytes appears yellow). Endothelial cells were stained using fluorescently labeled anti-CD31 antibody. Scale bars are 100 µm. (C) SD-IVM of the mouse liver 24 h after injection of

fluorescently labeled albumin shows dotted structure colocalizing with endothelial staining. Kupffer cells and endothelial cells were stained using fluorescently labeled anti-F4/80 and anti-CD31 antibody, respectively. Scale bars are 33 μm . **(D)** 1,704 interactions of platelets with 124 Kupffer cells were tracked over 30 min using Imaris software, and the dwell time was plotted. **(E)** Average platelet interactions per Kupffer cell per 30 min, grouped by dwell time. Data represent means \pm SEM. **(F)** Interactions of platelets with a single Kupffer cell are visualized using SD-IVM of the mouse liver. While most interactions are transient, a small proportion (arrows) forms firm interactions. Kupffer cells and endogenous platelets were stained using fluorescently labeled anti-F4/80 and anti-CD49b antibody, respectively. Scale bars are 8 μm . **(G)** 3D reconstruction of a single Kupffer cell of naive CD41-YFP^{ki/+} mice based on a z-stack obtained using SD-IVM of the liver. The Kupffer cell was labeled using an anti-F4/80 antibody. Note the YFP platelet remnant (bright green) inside the Kupffer cell (arrows). Scale bars are 100 μm . **(H)** Percentage of Kupffer cells (KCs) in CD41-YFP^{ki/+} mice that harbor platelet-YFP remnants inside. Results from all experiments shown are representative of three independent experiments.

albumin initially showed prominent staining within the blood vessels (Fig. S1 A and Video 1) and after 24 h ended up in a patchy distribution in endothelium (Fig. 1 C). Clearly, this imaging allows discrimination between the three compartments: Kupffer cells, hepatocytes, and endothelium. This enabled us to follow the fate of unperturbed platelets as well as aged and desialylated platelets in the mouse liver and to pinpoint the exact location of their clearance.

We first tracked endogenous platelets using intravital microscopy (IVM) to ensure that desialylated platelets experienced the same fate as unperturbed old platelets. Under basal conditions, platelets frequently attached to Kupffer cells in a touch-and-go fashion, rapidly releasing back into the bloodstream. However, a small population of platelets persistently stuck to Kupffer cells (Fig. 1, D–F; and Video 2). Using image analysis software to quantify these interactions, we found that, on average, every Kupffer cell forms firm adhesion (dwell time \geq 20 min) with 0.85 platelets per 30 min. While this may seem rather infrequent, with \sim 10–20 million Kupffer cells (Smedsrød et al., 1985; Bouwens et al., 1986; Hendriks et al., 1990; Wisse et al., 1996), and using the more conservative value of 10 million, this leads to \sim 408 million platelets cleared every day, well within the predicted daily platelet turnover in a mouse.

To confirm our findings in a model with endogenously labeled platelets, we made use of CD41-YFP^{ki/+} mice, in which a fraction of megakaryocytes and platelets express YFP (Zhang et al., 2007). Indeed, using IVM in these mice, we observed a small percentage of platelets stuck to Kupffer cells (Video 3). To investigate whether these firm adhesions translated to phagocytosis, we further examined the fate of these platelets using three-dimensional (3D) reconstructions. Platelet-YFP remnants were noted inside Kupffer cells (Fig. 1 G and Video 4). Fig. 1 G uses opacity to demonstrate that the platelets, which are difficult to see, become visible as the Kupffer cell membrane's translucence is increased, confirming their intracellular localization. We found that 39% of Kupffer cells in CD41-YFP^{ki/+} mice harbor YFP remnants inside (Fig. 1 H), with the caveat that only \sim 20% of platelets are YFP⁺, underestimating the number of Kupffer cells that likely took up platelets. Since only a small number of megakaryocytes were also YFP⁺ (Zhang et al., 2007), we believe that the YFP⁺ platelets represent the full spectrum of platelets and not platelets of a specific age. Indeed, nucleic acid/RNA profiles were equivalent in YFP⁺ and YFP⁻ platelets (a measurement of age). Hence, the capture and phagocytosis of aged platelets by Kupffer cells is an ongoing process that maintains normal levels of platelets and prevents old platelet accumulation in blood.

Kupffer cell-depletion causes accumulation of old platelets

We speculated that if Kupffer cells are crucial for the removal of aged platelets, eliminating the former would lead to the accumulation of old platelets in the bloodstream. We therefore gave mice a single liposomal clodronate injection, which is known to deplete Kupffer cells for \sim 1 wk, and followed the platelet population over time. We observed a significant shift of the total platelet population toward higher galactose exposure, which reached its peak at \sim 3 d, but then leveled out (Fig. 2, A and B). Importantly, as Kupffer cells started to return after 7 d following depletion (Fig. S1 B), galactose levels on platelets began returning toward control levels by day 10. Interestingly, this was accompanied by a 30% reduction in the percentage and 25% reduction in the absolute numbers of young (reticulated, enriched for nucleic acids, particularly RNA [Kienast and Schmitz, 1990; Harrison et al., 1997]) platelets (Fig. 2, C and D; and Fig. S1 C), suggesting a well-controlled feedback loop. Overall, there was a significant increase in the total number of platelets following Kupffer cell depletion (Fig. 2 E and Fig. S1 D), in line with previous studies (Stritt et al., 2017). For further confirmation and a more direct observation of platelet aging in vivo, we labeled platelets with an anti-GPIIb β antibody in vivo and compared galactose exposure of labeled “old” and unlabeled control platelets 3 d later. We observed a significant shift in the galactose exposure on the labeled platelets (Fig. S1 E), which is in line with our own data after Kupffer cell depletion (Fig. 2 B) as well as previous reports that platelets become desialylated as they circulate (Grozovsky et al., 2015a). These results revealed three things: (i) Kupffer cell depletion abolished the capacity to remove endogenous (un-manipulated) aged platelets from the circulation, causing them to accumulate; (ii) simultaneously, production of new platelets was reduced, which in combination led to a (iii) moderate increase in platelet count, indicating that feedback mechanisms tightly regulate platelet mass (Kaushansky et al., 1994; Gurney et al., 1994; Kaushansky, 2005) and prevent excessive platelet production.

Desialylated platelets rapidly adhere to Kupffer cells

To determine whether desialylation mimics endogenous removal of platelets, we infused ex vivo desialylated labeled platelets into mice. These platelets rapidly accumulated on Kupffer cells in very large numbers, whereas transfused control platelets did not accumulate and continued circulating (Fig. 3, A and B; and Video 5). As such, we used this system with more abundant events to further study the molecular mechanisms of platelet clearance by Kupffer cells. Depleting Kupffer cells by clodronate liposome pretreatment almost completely abolished adherence

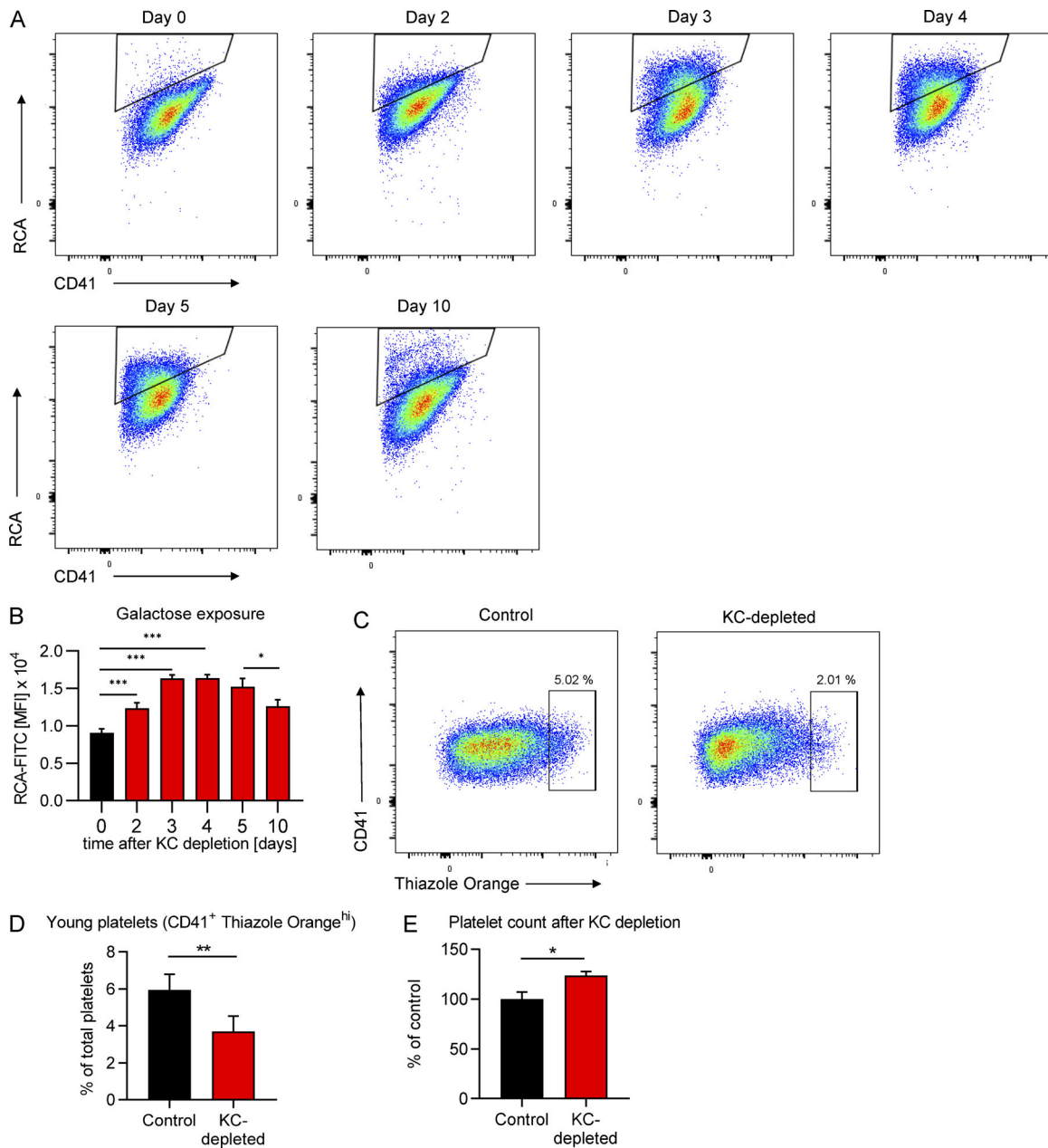


Figure 2. Kupffer cells are central to the removal of desialylated platelets under homeostatic conditions. Mice were Kupffer cell depleted using clodronate liposomes, and the platelet population was followed over time. **(A)** Representative flow cytometry plots showing a shift in the total platelet population toward higher galactose expression over time. **(B)** Quantification of the galactose exposure in the total platelet population over time. Data represent means \pm SEM ($n = 5$ mice/d). MFI, mean fluorescence intensity. **(C)** Representative flow cytometry plots showing the change in CD41⁺ Thiazole Orange^{hi} young platelet population in the blood of control mice and mice on day 5 after Kupffer cell depletion. **(D)** Quantification of the CD41⁺ Thiazole Orange^{hi} young platelet population in the blood from control mice and mice on day 5 after Kupffer cell depletion. Data represent means \pm SEM ($n = 5$ mice per group). **(E)** Total platelet count was analyzed using flow cytometry of blood from control mice and mice on day 5 after Kupffer cell depletion. Data represent means \pm SEM ($n = 5$ mice per group). One-way ANOVA with post-hoc testing (B) and unpaired two-tailed *t* test (D and E) were used to determine statistical significance. *, $P < 0.05$; **, $P < 0.01$; ***, $P < 0.001$. Results from all experiments shown are representative of at least three independent experiments. KC, Kupffer cell.

of ex vivo desialylated platelets in liver sinusoids (Fig. 3, A and B; and Video 6). To avoid any untoward effects of isolating platelets ex vivo, sialidase (neuraminidase) was injected i.v. Once again, platelets adhered avidly to Kupffer cells, reaching maximum levels around 10–20 min after injection (Fig. 3, C and D; and Video 7). Colocalization analyses revealed that the vast majority of desialylated platelets accumulated on Kupffer cells, while only

a small fraction showed adhesion to the endothelium (Fig. 3 E). Importantly, binding of platelets to hepatocytes was negligible. We also confirmed this using mice with endogenously labeled platelets (CD41-YFP^{ki/+} mice; Fig. S1, F and G). While interactions with endothelium did occur, this was a much rarer event and never led to rolling interaction (i.e., only touch-and-go interactions were observed). It was impossible to determine whether

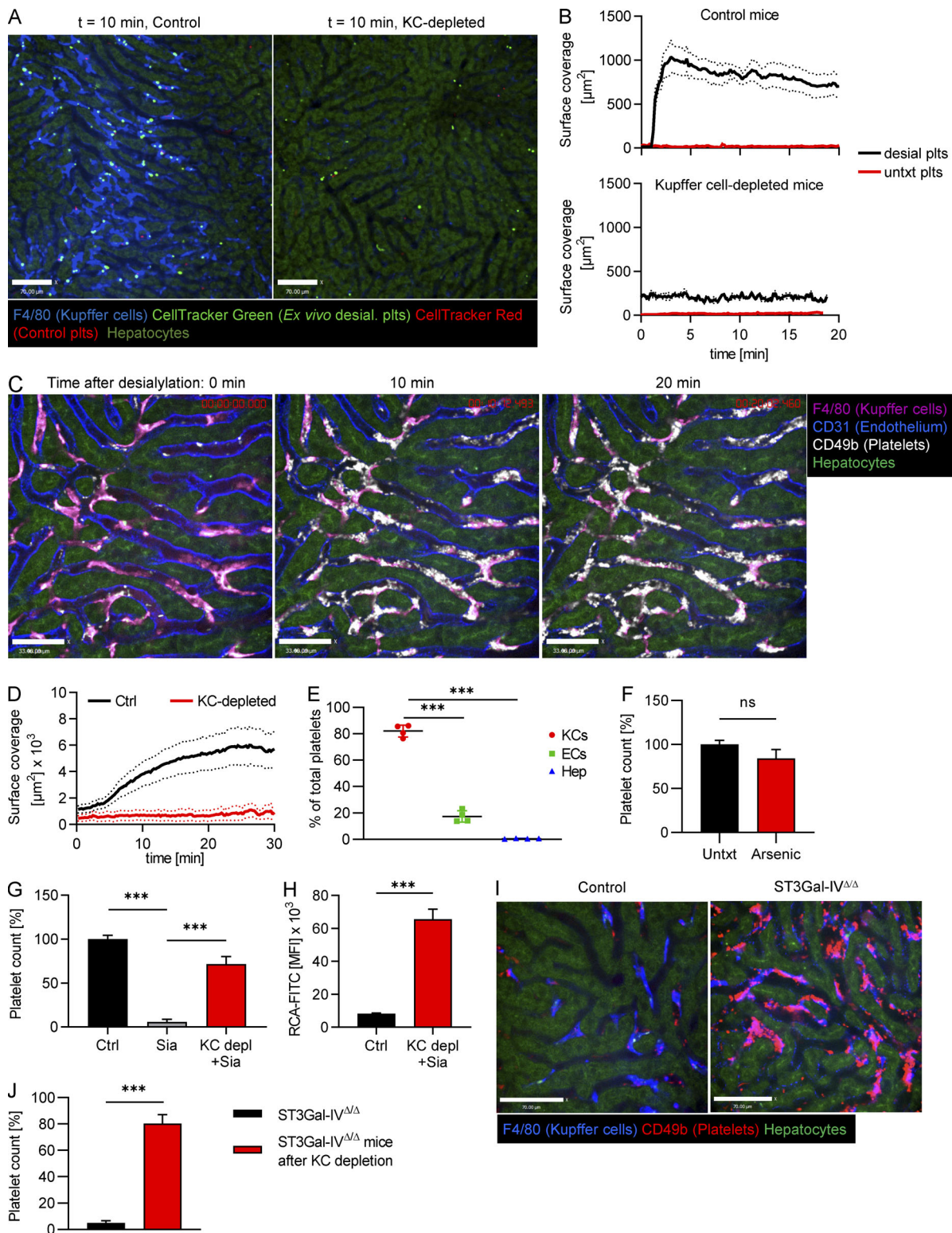


Figure 3. Desialylated platelets rapidly accumulate on Kupffer cells. (A) Ex vivo desialylated (desial. plts) and untreated control platelets were labeled with CellTracker Green and Red dye, respectively, and transfused into control and Kupffer cell–depleted mice. Representative still images from videos obtained using SD-IVM of the mouse liver. Scale bars are 70 μm . (B) Quantification of the accumulation of ex vivo desialylated platelets and untreated (untxt) control platelets in wild-type and Kupffer cell–depleted mice. $n = 3$ mice per group. (C) SD-IVM of the liver of mice treated with 50 mU sialidase. Representative still images obtained at the indicated time points. Kupffer cells, endothelial cells, and endogenous platelets were stained using fluorescently labeled anti-F4/80, anti-CD31, and anti-CD49b antibody, respectively. Scale bars are 33 μm . (D) Quantification of the accumulation of platelets within the first 30 min after treatment with 50 mU sialidase in control (Ctrl) and Kupffer cell (KC)–depleted mice. $n = 5$ mice per group. (E) Colocalization of platelets with Kupffer cells, endothelial cells (ECs), and hepatocytes (Hep) was quantified at the 20-min time point after sialidase treatment using Imaris software. Data represent means \pm SEM

($n = 4$ mice per group). **(F)** Platelet count was measured using flow cytometric analysis of blood from control mice as well as mice treated with 250 parts-per-billion (ppb) arsenic in drinking water for 5 wk to specifically cause defenestration of the liver sinusoidal endothelial cells. Data represent means \pm SEM ($n = 5$ mice per group). **(G)** Platelet count was measured using flow cytometric analysis of blood from control mice, control mice treated with sialidase, and Kupffer cell-depleted (using clodronate liposomes) mice treated with sialidase. Measurement was performed 24 h after sialidase application. Data represent means \pm SEM ($n = 4$ mice per group). **(H)** Galactose exposure on platelets of untreated control mice and Kupffer cell-depleted (using clodronate liposomes) mice treated with sialidase was measured using flow cytometry. Data represent means \pm SEM ($n = 3$ mice per group). **(I)** SD-IVM of the liver of control and ST3Gal-IV $^{\Delta/\Delta}$ mice shows massive accumulation of platelets on Kupffer cells of ST3Gal-IV $^{\Delta/\Delta}$ mice already under steady-state conditions. Scale bars are 70 μ m. **(J)** Platelet count was quantified using flow cytometry of blood from ST3Gal-IV $^{\Delta/\Delta}$ mice before and 5 d after Kupffer cell depletion using clodronate liposomes. Platelet count is expressed relative to untreated wild-type controls. Data represent means \pm SEM ($n = 4$ mice per group). One-way ANOVA with post-hoc testing (E and G) and unpaired two-tailed t test (F, H, and J) were used to determine statistical significance. *, $P < 0.05$; **, $P < 0.01$; ***, $P < 0.001$. Results from all experiments shown are representative of at least three independent experiments.

this interaction was with endothelium or with hepatocyte microvilli protruding through the fenestrae (seen only by electron microscopy [EM]), a proposed but never-tested mechanism (Li et al., 2017). To further confirm that hepatocytes or their protrusions into the liver sinusoids do not play a role in removal of aged platelets, as has recently been suggested, we treated mice with highly diluted arsenic in their drinking water. As described previously (Guidotti et al., 2015; Straub et al., 2007), this significantly reduces the number of fenestrations in liver sinusoidal endothelial cells, preventing the ability of hepatocytes to reach across the space of Disse and interact with circulating intravascular cells. Treatment with arsenic in this manner did not affect platelet counts, clearance of desialylated platelets, or the number or size of Kupffer cells in mice (Fig. 3 F and Fig. S2, A and B), but reduced the number of fenestrations as assessed by EM (Fig. S2, C and D), indicating that hepatocytic microvilli most likely do not contribute to the tethering of the platelets to the endothelium or removal of old platelets from the bloodstream under homeostatic conditions.

In mice pretreated with clodronate liposomes to deplete Kupffer cells, platelet accumulation after sialidase treatment was virtually absent (Fig. 3 D), indicating that the Kupffer cell is the major cell type responsible for this process. When we measured the peripheral platelet count in mice 24 h after sialidase treatment using flow cytometry, it was at \sim 5% of the level of control mice (Fig. 3 G), validating the imaging data. Kupffer cell depletion prevented the massive drop in platelet count after sialidase treatment (\sim 70% of control levels). Platelets that were circulating in Kupffer cell-depleted mice treated with sialidase showed substantially increased galactose exposure (Fig. 3 H), indicating that desialylated platelets circulate in the bloodstream in the absence of Kupffer cells. As i.v. clodronate treatment also affects macrophages in the spleen, and to exclude the possibility that highly vascularized organs like the lung are involved, we investigated the role of splenic macrophages and the lung vasculature in platelet clearance. Imaging the spleen and lung revealed only basal levels of platelet binding, and we did not observe significant additional accumulation of platelets upon sialidase treatment (Fig. S3, A and B; and Video 8). Further confirmation for the noninvolvement of the spleen in the removal of desialylated platelets came from our finding that platelet counts in splenectomized mice went down to 5% 24 h after sialidase treatment, very similar to our observations in control mice (Fig. S3 C). While these data point to an important role of the liver in the removal of desialylated platelets and

suggest only a minor or no role for the spleen, we cannot rule out that the liver compensates when the spleen is removed. We were also interested if bone marrow macrophages would phagocytose desialylated platelets. To this end, we injected desialylated labeled platelets into mice and flushed out their bone marrow 1 h later. Using flow cytometry and microscopy, we did not observe uptake of desialylated platelets by bone marrow macrophages (Fig. S3, D and E).

Defective endogenous sialylation causes massive platelet accumulation on Kupffer cells

Patients with mutations in the *GNE* gene encoding for glucosamine (UDP-*N*-acetyl)-2-epimerase/*N*-acetylmannosamine kinase, an enzyme involved in sialic acid biosynthesis (Futterer et al., 2018; Revel-Vilk et al., 2018), as well as patients with a mutation in the gene coding for the sialic acid transporter SLC35A1 (Kauskot et al., 2018) have severe thrombocytopenia and bleeding disorders. To explore the fate of platelets with defective endogenous sialylation, we next examined mice deficient in ST3Gal-IV sialyltransferase (ST3Gal-IV $^{\Delta/\Delta}$) that display a bleeding phenotype, a reduction in plasma vWF levels, and thrombocytopenia (Ellies et al., 2002). Using SD-IVM, we found that ST3Gal-IV $^{\Delta/\Delta}$ mice showed massive accumulation of endogenous platelets on Kupffer cells under basal homeostatic conditions and a distinct reduction in the number of circulating platelets to 5% of control levels (Fig. 3, I and J; and Video 9). Depleting Kupffer cells of ST3Gal-IV $^{\Delta/\Delta}$ mice using clodronate liposomes restored their platelet counts to 80% of control levels (Fig. 3 J), underlining the crucial importance of Kupffer cells in the removal of endogenously desialylated platelets. Of note, Kupffer cells from ST3Gal-IV $^{\Delta/\Delta}$ mice showed unaltered size, number, and function compared with control mice (Fig. S4).

After adhesion, desialylated platelets are phagocytosed by Kupffer cells

Platelets that attached to Kupffer cells were next tracked over time. Quantification of the amount of platelets adhering to Kupffer cells at 30 min and 24 h after sialidase treatment revealed a 10-fold decrease in the number of adherent platelets over this time frame (Fig. S5 A). Cytoplasmic CellTracker Red dye-labeled desialylated platelets that bound to Kupffer cells began to release dye inside the cell body of the Kupffer cells at \sim 40 min (Fig. 4, A and D; and Videos 10 and 11). We confirmed this finding in vitro using isolated Kupffer cells and platelets (Fig. S5, B and C). To determine whether the platelets were

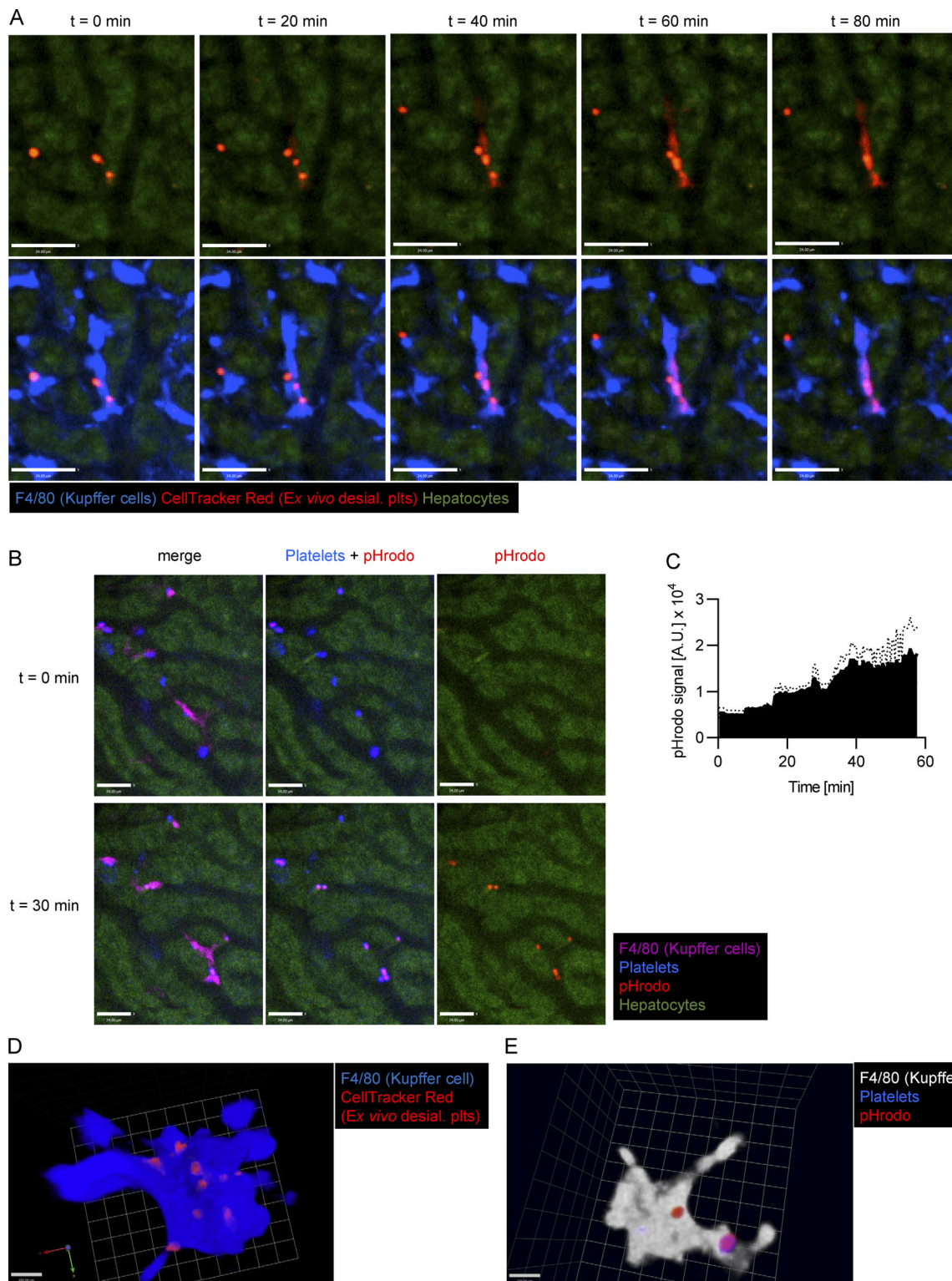


Figure 4. **Kupffer cells phagocytose desialylated platelets.** (A) SD-IVM of the liver of wild-type mice i.v. injected with desialylated platelets labeled with CellTracker Red dye. Representative images taken at the indicated time points. Kupffer cells were labeled using an anti-F4/80 antibody. Note how the CellTracker dye leaks from the platelet into the Kupffer cell body, thereby turning it red. Scale bars are 34 μm . (B) SD-IVM of the liver of wild-type mice i.v. injected with desialylated pHrodo-labeled platelets. Representative images taken at the indicated time points. Kupffer cells were labeled using an anti-F4/80 antibody. Scale bars are 34 μm . (C) Quantification of the pHrodo signal over time from four mice injected with pHrodo-labeled platelets. A.U., arbitrary unit. (D) 3D reconstruction of a Kupffer cell after injection of CellTracker Red-labeled platelets. Scale bar is 100 μm . (E) 3D reconstruction of a Kupffer cell after injection of pHrodo-labeled platelets. Scale bar is 100 μm . Results from all experiments shown are representative of at least three independent experiments.

taken up and transferred to the phagolysosome for destruction, we labeled desialylated platelets with pHrodo, a pH-sensitive dye that serves as a specific sensor of phagocytosis (Sureward and Kubes, 2017). Upon injection of platelets into mice, they immediately bound Kupffer cells, and within 30 min, a strong pHrodo signal was detected (Fig. 4, B and E; and Video 12), consistent with platelet phagocytosis and placement into low pH lysosomes by Kupffer cells.

Integrin α_M (CD11b/Mac-1) is not involved in the clearance of platelets through Kupffer cells

Next, we were interested to find out which receptors on Kupffer cells mediate binding and phagocytosis of desialylated platelets. Since $\alpha_M\beta_2$ was found to be involved in the clearance of transfused platelets after cold storage (Hoffmeister et al., 2003a), we investigated if it also plays a role during clearance of desialylated endogenous platelets. However, when we treated Mac1-deficient mice with sialidase, there was no difference in the accumulation of desialylated platelets on Kupffer cells compared with control mice, as shown by IVM (Fig. S5 D).

AMR on Kupffer cells is insufficient for old platelet clearance

The AMR is a member of the C-type lectin family of receptors involved in recognition, binding, and clearance of desialylated proteins (asialoglycoproteins; Ashwell and Morell, 1974). AMR has also been reported to be involved in the clearance of desialylated platelets generated following cold exposure or by bacterial sialidase activity during sepsis (Rumjantseva et al., 2009; Grewal et al., 2008). While AMR was difficult to detect on Kupffer cells in the past, more recently an unbiased single-cell transcriptomic study (Tabula Muris Consortium, 2018), a mass spectrometry-based proteomics study, and our own data using flow cytometry (Fig. S5 E) confirmed the existence of AMR on Kupffer cells, along with the clathrin-mediated endocytosis machinery needed for the uptake of desialylated platelets (Azimifar et al., 2014). Previous studies used asialofetuin (ASF) to block the AMR to demonstrate complete prevention of platelet clearance (Li et al., 2015; Xu et al., 2018). However, AMR-deficient mice had less-convincing results (Grewal et al., 2008; Li et al., 2017), suggesting that ASF blocked more than AMR. Using imaging, desialylated platelet accumulation on Kupffer cells was significantly reduced in mice pretreated with ASF compared with control mice (Fig. 5, A [panel II] and B; and Videos 13 and 14). *Asgr1*^{-/-} mice, which lack the major AMR subunit (Braiterman et al., 1989; Bider et al., 1995) that received sialidase, had similar levels of platelet accumulation on Kupffer cells as wild-type mice (Fig. 5, A [panel III] and B; and Video 15), in line with *Asgr1*^{-/-} mice showing normal platelet counts (Fig. S5 F). These results suggest that ASF does not specifically inhibit the AMR but also likely inhibits additional asialoglycoprotein receptors.

MGL is a novel receptor that aids AMR on Kupffer cells for the clearance of desialylated platelets

Recent work has reported that MGL, which mediates the clearance of vWF (Ward et al., 2018), was also blocked by ASF

(Ng et al., 2014). We confirmed the expression of MGL on murine Kupffer cells (Fig. S5 G). Blocking MGL1/2 had no effect on the accumulation of desialylated platelets on Kupffer cells (Fig. 5, A [panel IV] and B; and Video 16). However, blocking MGL1/2 in *Asgr1*^{-/-} mice essentially abolished the binding of desialylated platelets to Kupffer cells (Fig. 5, A [panel V] and B; and Video 17). These data suggest that MGL and the AMR together clear aged platelets. To translate this work to humans, we investigated whether human MGL also bound to desialylated human platelets. Flow cytometry revealed that desialylated human platelets bound significantly more fluorescently labeled recombinant human MGL than control platelets (Fig. S5, H and I), indicating that the binding of MGL to desialylated platelets might also be relevant in humans.

Increased levels of old platelets impair hemostasis

The fact that we clear billions of platelets a day suggests that poor clearance would lead to deficient platelet function. To know what the consequence of accumulating desialylated platelets in the bloodstream was and if these platelets were still able to perform their primary function (to maintain hemostasis), we examined the platelets of wild-type mice 5 d after Kupffer cell depletion, when the shift of the platelet population to higher galactose levels was at its maximum (Fig. 2, A and B). Under resting conditions, platelets from Kupffer cell-depleted animals showed higher exposure of P-selectin (a marker of α -granule release) compared with control platelets, indicating partial degranulation already in the steady state (Fig. 6 A). We next chose to stimulate platelets with thrombin, which acts through the protease-activated receptors 3 and 4 (Offermanns, 2006). Platelets from Kupffer cell-depleted mice were nonresponsive to low levels of thrombin, as we did not observe a change in P-selectin exposure over the resting state. Only with high concentrations of thrombin did we see increased P-selectin levels over the resting state; however, it was still lower than mice with normal levels of Kupffer cells. We next investigated the ability of platelets to activate their α IIb β 3 integrin, which is essential for fibrinogen binding and stable aggregate formation. Following stimulation with thrombin, platelets from Kupffer cell-depleted mice showed severely reduced α IIb β 3 activation (Fig. 6 B). Taken together, these results show that platelets from Kupffer cell-depleted mice are partially degranulated even without stimulation and less responsive to thrombin stimulation. We next analyzed the capacity of the platelets to aggregate and found that while control platelets formed stable aggregates after thrombin stimulation, platelets from Kupffer cell-depleted animals were unable to do so and in fact showed significantly less platelet aggregation (Fig. 6 C). Importantly, the aggregates formed by platelets from Kupffer cell-depleted mice were also much more unstable (Fig. 6, D and E).

Next, we asked what the consequence of the observed defects for hemostasis in vivo would be and therefore subjected wild-type mice on day 5 after Kupffer cell depletion to the tail bleeding time assay. All Kupffer cell-depleted mice tested were unable to stop bleeding during the 20-min observation period,

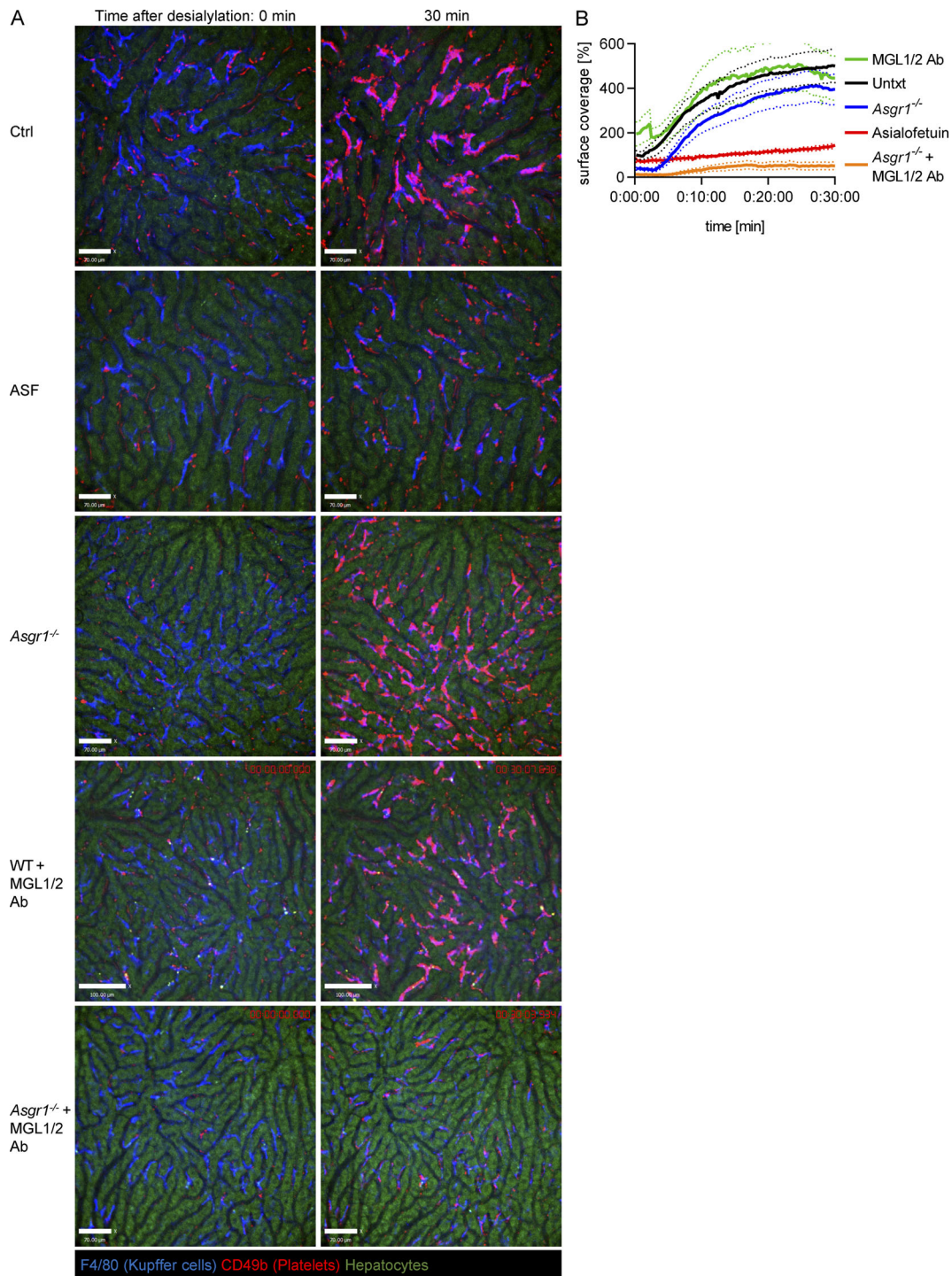


Figure 5. **A collaboration between MGL and AMR facilitates binding of desialylated platelets to Kupffer cells.** (A) SD-IVM was performed on the liver of control mice, mice treated with ASF, *Asgr1*^{-/-} mice, wild-type mice treated with MGL1/2 blocking antibody (Ab), and *Asgr1*^{-/-} mice treated with MGL1/2 blocking antibody after injection of 50 mU sialidase. Kupffer cells and platelets were labeled using anti-F4/80 and anti-CD49b antibodies, respectively. Representative images taken at the indicated time points. Scale bars are 70 μ m, except for the WT+MGL1/2 antibody images, where scale bars are 100 μ m. (B) Quantification of platelet accumulation shown in A with $n \geq 4$ mice per group, normalized to control mice values. Results from all experiments shown are representative of at least three independent experiments.

while 80% of control mice stopped bleeding in <6 min (Fig. 6 F). Kupffer cell-depleted wild-type mice also showed a more than fourfold increase in the amount of blood lost during the experiment compared with controls (Fig. 6 G). These results indicate

that shifting the distribution of platelet age toward older platelets after Kupffer cell depletion is sufficient to reduce activation and aggregation capacity and translates into a significant defect in maintaining hemostasis.

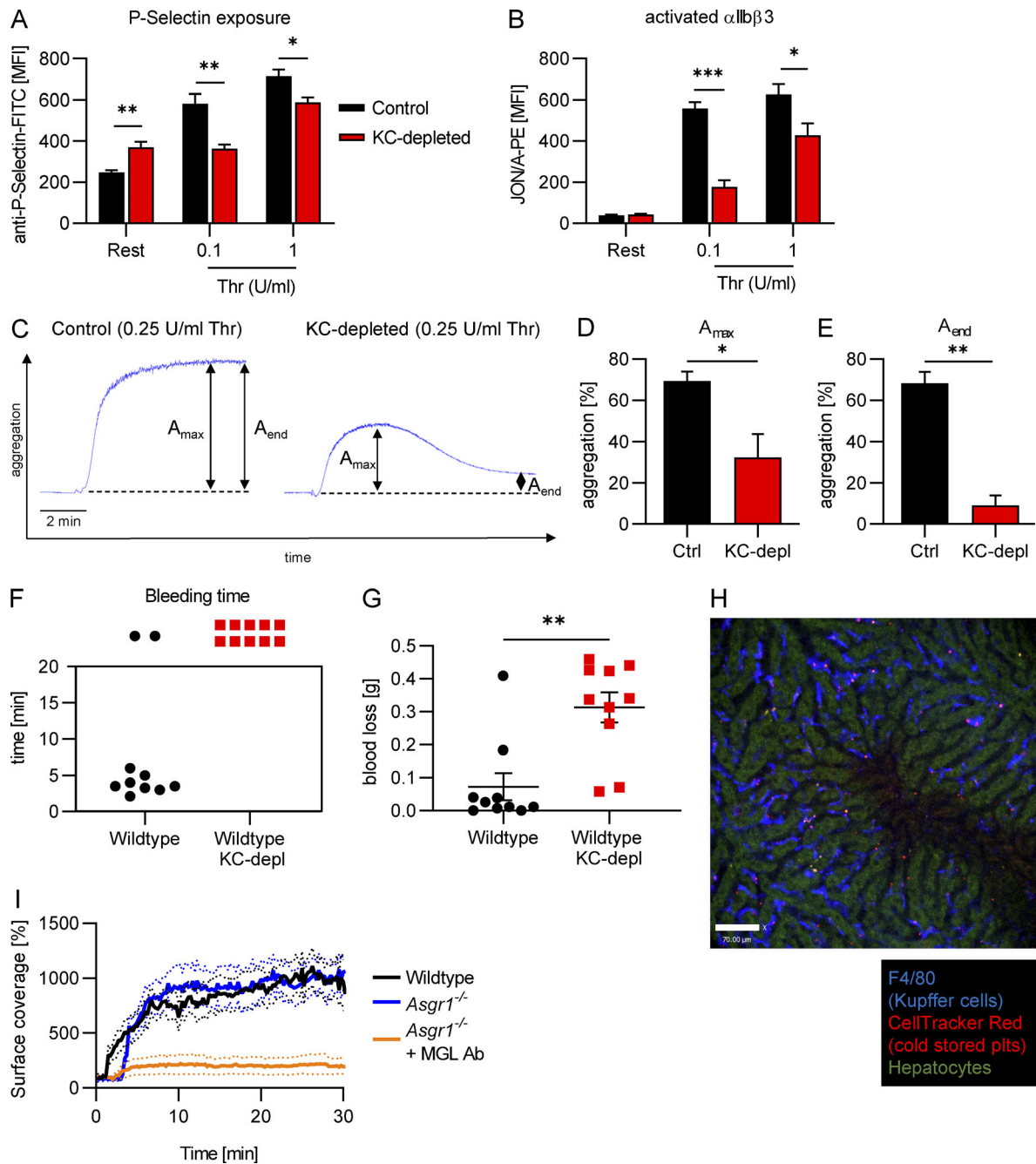


Figure 6. Old platelets show significantly reduced hemostatic capacity. (A and B) Flow cytometric analysis of platelets from mice 5 d after Kupffer cell depletion shows increased P-selectin exposure in resting conditions, but decreased P-selectin exposure after stimulation with thrombin (Thr) compared with control platelets (A) and significantly reduced $\alpha\text{IIb}\beta\text{3}$ integrin activation (JON/A-PE binding; B) after stimulation with thrombin. Data represent means \pm SEM ($n = 5$ mice per group). (C) Representative aggregation traces of platelets isolated from control mice or mice 5 d after Kupffer cell depletion stimulated with 0.25 U/ml thrombin. (D and E) Maximum aggregation (A_{max} ; D) and aggregation at the end time point (A_{end} ; E) of platelets isolated from control mice or mice 5 d after Kupffer cell depletion. Data represent means \pm SEM ($n = 3$ mice per group). Control mice and mice 5 d after Kupffer cell depletion were subjected to the tail bleeding time assay. (F) Time until bleeding cessation; values >20 min indicate that bleeding did not stop within the 20-min observation period of the experiment. (G) Quantification of the amount of blood loss. Data represent means \pm SEM ($n = 10$ mice per group). (H) SD-IVM was performed on the liver of control mice after injection of cold-stored platelets. Kupffer cells and platelets were labeled using anti-F4/80 and CellTracker Red dye, respectively. Representative image taken at 30 min after injection. Scale bar is 70 μm . (I) Quantification of the accumulation of cold-stored platelets in wild-type and *Asgr1*^{-/-} mice as well as *Asgr1*^{-/-} mice treated with MGL-blocking antibody. $n \geq 4$ mice per group, normalized to control mice values. Unpaired two-tailed t test (A, B, D, E, and G) was used to determine statistical significance. *, $P < 0.05$; **, $P < 0.01$; ***, $P < 0.001$. Results from all experiments shown are representative of at least three independent experiments.

Blockade of MGL and AMR reduces binding of cold-stored platelets to Kupffer cells

Further, we wanted to investigate if our findings also extend to the cold storage phenomenon. We therefore used intravital imaging to study the fate of platelets transfused after 24 h of cold storage and found them to accumulate on Kupffer cells (Fig. 6 H), very similar to desialylated platelets (Fig. 3 A). We next asked if it would be possible to prevent their binding to Kupffer cells using our approach of combined blockade of AMR and MGL. Indeed, binding of cold-stored platelets to Kupffer cells was reduced in *Asgr1*^{-/-} mice treated with MGL-blocking antibody compared with *Asgr1*^{-/-} or wild-type mice (Fig. 6 I).

Discussion

Desialylated platelets (by enzyme or bacteria), transgenic mice that have desialylated platelets, cooled platelets (for 2 h), or prolonged refrigeration of platelets all lead to platelet depletion by varied mechanisms, including hepatocytes, hepatocyte villi poking through sinusoidal endothelial fenestrae (Li et al., 2017), Kupffer cells (Sørensen et al., 2009), or hepatocytes collaborating with Kupffer cells. The AMR has been extensively studied as the receptor for catching desialylated platelets (Grewal et al., 2013; Grozovsky et al., 2015a), and the results suggest that there are additional receptors. While it is tempting to extend this body of work to platelet clearance in normal homeostatic processes, no studies have visualized endogenous platelet clearance, resulting in speculation as to the mechanism. Indeed, in our study we followed the fate of endogenous platelets and observed that the Kupffer cells scan all the platelets as they flow through the main stream of blood. We observed touch-and-go interactions continuously under basal conditions. On average, a platelet would firmly adhere to a Kupffer cell once every 35 min. Because of the vast number of Kupffer cells in the liver, this accounted for massive removal of platelets every day. Because of the rarity of this process, we also desialylated platelets in vivo and examined platelets that had a mutation in the sialic acid transferase necessary for addition of sialic acid onto the surface of platelet proteins and noted similar Kupffer cell-dependent platelet clearance. Depleting Kupffer cells using clodronate prevented the sequestration of desialylated platelets but also caused a striking accumulation of desialylated platelets in the vasculature. These findings provide evidence that Kupffer cells play a central role in the removal of desialylated platelets under homeostatic conditions. Our findings in the context of this in vivo system are consistent with but extend upon previous studies of platelets and AMR (Li et al., 2016; Hoffmeister and Falet, 2016; Grozovsky et al., 2015b) to invoke a role for a second key receptor, MGL. Using our established SD-IVM setup, we were able to precisely follow the fate of desialylated platelets and show that Kupffer cells play an important role in platelet removal under homeostatic conditions. While a very small percentage of platelets also bound endothelium, their fate requires further investigation.

Recently, a publication reported that desialylation leads to removal of transfused platelets by a two-step mechanism in which platelets adhere to and then roll on hepatocyte microvilli

by interacting with the AMR, followed by their capture through the CLEC4F receptor on Kupffer cells (Li et al., 2017). In our study, using state-of-the-art SD-IVM with high spatiotemporal resolution, we did not observe deceleration or rolling of platelets on hepatocytes but rather direct capture by Kupffer cells. It is worth noting that previous work reported that hepatocyte pseudopods could extend through the fenestrae and that lymphocytes could reach their pseudopods across this barrier to kill infected hepatocytes (Guidotti et al., 2015), suggesting cross-talk between hepatocytes and the intravascular compartment. While we cannot discount that the small percentage of platelets that did touch down on endothelium were cleared by a hepatocyte-dependent mechanism, our imaging revealed a far more prevalent interaction of platelets directly with Kupffer cells. Eradicating liver endothelial cell fenestrations by an established technique of treating the mice with highly diluted arsenic in their drinking water (Guidotti et al., 2015; Straub et al., 2007) did not significantly impact the platelet count, indicating that hepatocytic microvilli are not a major mechanism for the removal of desialylated platelets from the bloodstream under homeostatic conditions. Moreover, the profound phenotype of mice lacking Kupffer cells, including decreased sequestration of desialylated platelets by the liver, an increase in circulating platelets, and remnants of platelets inside Kupffer cells but not hepatocytes, strongly implicates this macrophage in platelet clearance. Platelet desialylation may also take place during platelet storage (Cho et al., 2018), indicating that our findings might provide new avenues to maintain transfused platelets in the circulation for longer periods of time.

We identified a new player in platelet clearance: MGL works together with the AMR to facilitate the binding and removal of desialylated platelets by Kupffer cells. There is limited available information regarding MGL in liver and even less regarding platelets. Recent work has reported that MGL mediates the clearance of vWF (Ward et al., 2018). Blocking both AMR and MGL prevented removal of desialylated platelets. While AMR was known to be highly expressed on hepatocytes, it was for many years thought not to be expressed on Kupffer cells. However, more recent unbiased approaches including single-cell transcriptomic studies verified that *Asgr1* is expressed by Kupffer cells (Tabula Muris Consortium, 2018). Moreover, mass spectrometry-based proteomics confirmed its existence in Kupffer cells, along with the clathrin-mediated endocytosis machinery needed for the uptake of desialylated platelets (Azimifar et al., 2014).

To date, rapid clearance of platelets leads to bleeding; however, whether any impairment exists when platelets are not cleared in a timely fashion remained unknown. When we investigated whether old platelets were functional, we found that they were significantly defective. Even more surprising, however, was the observation that delaying clearance of platelets by 5 d also was sufficient to increase bleeding times. Although many of the platelets still had some sialic acid content, clearly the overall shift was sufficient to impair clotting. Our findings are consistent with a recent report that investigated the role of intrinsic apoptosis in platelet lifespan and function and found that BAK/BAX-deficient mice exhibited increased bleeding times (Pleines et al., 2018). It appears that both apoptosis and

desialylation set a timer on platelet lifespan to maintain a healthy, functional platelet population. However, at this time it is unknown how apoptotic platelets are cleared from circulation. While it is tempting to speculate that apoptotic platelets might be cleared by Kupffer cells in the liver as well, this clearly requires more investigation.

Our observations may be relevant to a number of disease states. For example, immune thrombocytopenia (ITP) is a bleeding disorder caused by autoantibodies against platelet glycoproteins GPIIb/IIIa (integrin α IIb β 3) or GPIb α . In ITP patients, platelets are thought to be cleared by splenic macrophages through an Fc γ R-dependent process; however, there are many cases that are refractory to treatment targeting Fc γ R and/or splenectomy. Many of these Fc γ R-independent cases are due to GPIb α autoantibodies. These anti-GPIb α antibodies were shown to induce sialidase to the surface of platelets, leading to platelet desialylation and clearance (Li et al., 2015). A recent case study reported that the sialidase inhibitor oseltamivir phosphate improved platelet counts of an ITP patient refractory to standard Fc γ R-dependent treatment (Shao et al., 2015). These data indicate that the platelet clearance pathway described herein might also be involved in the increased platelet clearance observed in a subset of ITP patients. Our findings that combined blockade of AMR and MGL reduces the accumulation of cold-stored platelets to Kupffer cells raises interesting follow-up questions that ultimately may lead to improved circulating times after transfusion for stored platelets.

Additionally, it is well established that a number of respiratory pathogens such as *S. pneumoniae* express sialidases as virulence factors that can desialylate platelets, resulting in the reduction of thrombotic damage during sepsis (Grewal et al., 2008, 2013). More recently, it was shown that dengue virus infection can also cause platelets to get cleared through desialylation (Riswari et al., 2019). Our findings therefore might provide new approaches to target the severe thrombocytopenia that often occurs during *S. pneumoniae* or dengue virus infections. As we have previously shown that platelets help to encase and disarm blood-borne pathogens (Wong et al., 2013; Deppermann and Kubes, 2018), increasing the platelet count during sepsis by targeting MGL and AMR on Kupffer cells might prove to be beneficial. However, this may only be beneficial short term, as our data suggest that a significant delay in platelet clearance may lead to impaired hemostatic function resulting in bleeding, the very problem that needs to be fixed.

Materials and methods

Mice

6- to 8-wk-old C57BL/6 mice were obtained from The Jackson Laboratory. CD41-YFP^{ki/+} mice (Zhang et al., 2007) were a generous gift from Dr. Kelly McNagny (University of British Columbia, Vancouver, Canada). All mice were housed in a specific pathogen-free, double-barrier unit at the University of Calgary, with access to water and pelleted food ad libitum. All experimental procedures were approved by the University of Calgary Animal Care Committee and were in compliance with the Canadian Council for Animal Care Guidelines.

Antibodies and reagents

Antibodies against F4/80 (BM8) and CD11b (M1/70) were obtained from eBioscience. Antibodies against Ly6G (1A8), CD45 (30-F11), and Ly6C (HK1.4) were from Biolegend. Antibodies against CD49b (clone HMa2), P-selectin (CD62P, clone RB40.34), and CD41 (MWRReg30) were purchased from BD Biosciences Pharmingen. The MGL1/2 (CD301a/b) and AMR (ASGR1, clone #352803) antibodies, as well as recombinant human MGL (CD301/CLEC10A), were obtained from R&D Systems and labeled with Alexa647 dye using a Microscale Protein Labeling Kit (Thermo Fisher Scientific). Fluorescein-labeled Ricinus Communis Agglutinin (RCA-FITC) was obtained from Vector Laboratories. JON/A-PE antibody used to detect activated integrin α IIb β 3 and X649, an anti-GPIb β antibody used to label platelets in vivo, were from Emfret Analytics.

ASF, Thiazole Orange, and sialidase (neuraminidase) from *Clostridium perfringens* were obtained from Sigma-Aldrich. RCA-FITC was obtained from Vector Laboratories. CellTracker Red and Green dyes were from Thermo Fisher Scientific. Clodronate liposomes were from <http://www.clodronateliposomes.org>.

Treatments

For Kupffer cell depletion, mice were treated i.v. with clodronate liposomes (0.01 ml/g body weight) 48 h before performing the experiments. For in vivo desialylation, mice were i.v. injected with 50 mU sialidase. ASF (0.2 mg/g body weight) was administered i.v. before sialidase injection, where indicated. For in vivo blockade of the MGL receptors, mice were i.v. injected with 50 μ g anti-MGL1/2 antibody.

Isolation, ex vivo desialylation, and labeling of platelets

Blood was collected in a tube containing 20 U/ml heparin, and platelet-rich plasma (PRP) was obtained by centrifuging twice at 300 *g* for 6 min. PRP was washed twice at 800 *g* for 5 min, and the pellet was resuspended in Tyrode's buffer supplemented with prostacyclin (0.1 μ g/ml) and apyrase (0.02 U/ml). Platelets were then resuspended in Tyrode's buffer and treated with 2.5 mU sialidase for 20 min at 37°C. Desialylation was confirmed by binding of RCA-FITC. Platelets were labeled with 2 μ M CellTracker Red or Green dye for 20 min at 37°C and washed twice with Tyrode's buffer. For experiments investigating the cold-storage phenomenon, platelets were subsequently stored at 4°C for 24 h.

Platelet aggregation

400 μ l of a washed platelet suspension (3×10^5 platelets/ μ l) in Tyrode's buffer containing 2 mM CaCl₂ were continuously stirred (1,200 rpm), and light transmission was recorded on a 700 Whole Blood/Optical Lumi-Aggregometer (Chrono-log). Agonists were added at the indicated concentrations to the platelet suspension. Light transmission was expressed as percentages, with buffer representing 100% transmission and washed platelet suspension 0% transmission, respectively.

SD-IVM of the liver, spleen, and lung

Mice were anesthetized using 10 mg/kg xylazine hydrochloride and 200 mg/kg ketamine hydrochloride, and livers, spleens, and lungs were prepared for IVM as previously described (Surewaard

and Kubes, 2017; Deniset et al., 2017; Thanabalasuriar et al., 2017). A jugular vein catheter was inserted to inject fluorescent antibodies and to maintain anesthesia. Image acquisition (liver and spleen) was performed using an inverted microscope (Olympus IX81) equipped with a focus drive (Olympus) and motorized stage (Applied Scientific Instrumentation) and fitted with a motorized objective turret equipped with 4×/0.16 UPLANSAPO, 10×/0.40 UPLANSAPO, and 20×/0.70 UPLANSAPO objective lenses. Image acquisition (lung) was performed with an upright microscope (BX51; Olympus) using a 20×/0.95W NA water XLUM Plan F1 objective. The microscopes were equipped with a confocal light path (Quorum Technologies WaveFx) based on a modified CSU-10 head (Yokogawa Electric Corporation). Kupffer cells, platelets, and the endothelium were visualized using fluorescently labeled antibodies. For each animal, platelet accumulation was recorded in three randomly selected fields of view. Sialidase was injected i.v. 2 min after image acquisition was started. Volocity software (PerkinElmer) was used to quantify platelet accumulation over time.

Quantification of platelet–Kupffer cell interactions under naive conditions

SD-IVM of the mouse liver was performed in naive mice with platelets and Kupffer cells labeled and videos recorded as described above. Videos were then imported into Imaris Image Analysis Software (Bitplane). A surface containing all Kupffer cells was created and converted into a masked channel. Platelets were identified using the “spot” function, and platelet spots that overlapped with the Kupffer cell surface were filtered. Interactions between platelets and Kupffer cells were tracked, and their dwell time was recorded.

Analysis of platelet colocalization after sialidase treatment

SD-IVM of the mouse liver was performed upon sialidase treatment, with endothelium, platelets, and Kupffer cells labeled, and videos were recorded as described above. Videos were then imported into Imaris Image Analysis Software (Bitplane). A surface containing all Kupffer cells was created and converted into a masked channel. Platelets were identified using the “spot” function, and platelet spots that overlapped with the Kupffer cell surface were filtered. To identify platelets bound to the endothelium, platelet spots that colocalized with endothelial signal were filtered. Similarly, platelets that colocalized with the hepatocyte signal were identified.

Kupffer cell isolation

Mouse Kupffer cells were isolated as previously described (Lee et al., 2010). In brief, the abdominal cavity of anesthetized mice was opened to cannulate the inferior vena cava. The liver was perfused first with Ca²⁺- and Mg²⁺-free HBSS, and then with HBSS containing 0.05% collagenase type IV (Worthington Biochemical Corp.), 0.025% pronase E (US Biological), and 0.02% DNase I (Roche Diagnostics) at a flow rate of 4 ml/min. After perfusion, the liver was removed and further digested in HBSS containing 0.009% collagenase type IV, 0.009% pronase E, and 0.02% DNase I at 37°C with shaking for 30 min. The cell suspension was passed through a 100-micron nylon filter and

centrifuged at 25 g for 5 min at room temperature to remove the hepatocytes. The supernatant was transferred to a new tube and centrifuged at 400 g for 10 min at 4°C. The cell pellet was resuspended in 17% iodixanol (Axis-Shield PoC) solution and centrifuged at 400 g for 15 min at 20°C. The band of non-parenchymal liver cells was obtained and washed twice. Red blood cell lysis was performed using ACK lysis buffer (Gibco) for 2 min.

Cell staining and flow cytometry

For determination of platelet count or platelet galactose exposure, 50 µl of heparinized blood was diluted 1:20 in Tyrode’s buffer and incubated for 15 min at room temperature with platelet-specific fluorophore-labeled antibodies or RCA-FITC and analyzed on a FACSCanto flow cytometer (BD Biosciences). For platelet activation studies, samples were washed twice in Tyrode’s buffer, resuspended in Tyrode’s buffer containing 2 mM CaCl₂, activated with agonists at the indicated concentrations, stained with P-selectin-FITC and JON/A-PE for 6 + 6 min at 37°C and room temperature, respectively, and analyzed on a FACSCanto flow cytometer.

For Kupffer cell analysis, single-cell suspensions of non-parenchymal liver cells were resuspended in staining buffer (phosphate buffered saline + 2% BSA) at a concentration of ~1 × 10⁷ cells/ml. Cells were blocked with Fc block reagents (Bio-XCell) for 10 min. Subsequently, dead cells were labeled using Ghost Dye red 710 (Tonbo Bioscience). After an additional washing step, fluorescent antibodies were added and incubated for 30 min on ice. Cells were subsequently washed and fixed with 1% paraformaldehyde at room temperature for 30 min. Cells were washed twice and resuspended in 200 µl of flow cytometry buffer and analyzed on a FACSCanto flow cytometer. After exclusion of doublets and dead cells, Kupffer cells were identified as CD45⁺, Ly6G⁻, F4/80⁺, Ly6C^{low}, CD11b⁺.

Quantification of “young”/reticulated platelets

The percentage of young reticulated platelets was determined using Thiazole Orange as described (Stritt et al., 2017; Kienast and Schmitz, 1990; Harrison et al., 1997). 50 µl of heparinized blood was diluted 1:20 in Tyrode’s buffer and incubated for 15 min at room temperature with platelet-specific antibodies and 1 µg/ml Thiazole Orange and analyzed by flow cytometry.

Kupffer cell in vitro phagocytosis assay

50,000 Kupffer cells were incubated with 500,000 desialylated platelets in 96-well plates in DMEM supplemented with 10% FCS. Kupffer cells and platelets were stained using F4/80 antibodies and CellTracker Red dye, respectively. Images were recorded during incubation at 37°C and 5% CO₂ using an IncuCyte ZOOM system (Essen BioScience) equipped for phase contrast and two fluorescent channels (green: excitation, 440–480 nm; emission, 504–544 nm; red: excitation, 565–605 nm; emission, 625–705 nm) and with a 20× air objective (NA 0.40). Image analysis was performed using ImageJ software.

Scanning EM

Sample preparation for scanning EM was performed as described (Warren et al., 2006). In brief, mice were euthanized,

and livers were perfused with fixation solution (1% glutaraldehyde, 4% paraformaldehyde, 2 mM CaCl₂, 2% (wt/vol) sucrose, and 0.1 M cacodylate buffer pH 7.4). Livers were excised, cut into small pieces, and fixed for an additional 1 h at 4°C. Fixed liver tissue was dehydrated and dried using ethanol and hexamethyl-disilazane series, respectively. Tissue was splutter-coated and examined using a FEI XL30 scanning electron microscope.

Bacterial strain, culture, and infection

Staphylococcus aureus strain MW2 was obtained from the Network on Antimicrobial Resistance in *S. aureus* and transformed with pCM29 (Pang et al., 2010) to constitutively express GFP (Surewaard et al., 2012). Bacteria were grown in brain heart infusion medium (+ 10 µg/ml chloramphenicol to maintain the plasmid) overnight with shaking at 37°C. Bacteria were subcultured without antibiotics until exponential growth was achieved (OD_{660 nm} = 1.0), washed, and resuspended in saline. Mice were infected by i.v. injection of 5 × 10⁷ CFUs, and staphylococcal catching by Kupffer cells was observed using SD-IVM as described above.

Tail bleeding time

Mice were anesthetized, and a 1-mm segment of the tail tip was removed using a scalpel. Tail bleeding was monitored by placing the tail tip into an Eppendorf tube filled with 1 ml of warmed saline. Bleeding was determined to have ceased when no bleeding was observed for >1 min. Experiments were stopped after 20 min, and the amount of blood loss was determined by weighing the Eppendorf tube.

Donor consent and human platelet isolation

Ethical approval for obtaining healthy human volunteer blood was provided by the research ethics committee of the University of Calgary in accordance with the Declaration of Helsinki, and each human subject provided informed consent. Whole blood was drawn from healthy donors who had not taken aspirin products for ≥48 h. Blood was collected via a 21G butterfly needle into a 30-ml propylene syringe. The first 1 ml of blood was discarded. Blood was transferred into 50-ml polypropylene tubes containing 1 ml of acid citrate dextrose for every 5 ml of blood and gently inverted to mix. Samples were centrifuged at 140 g for 10 min at room temperature, and the upper layer (PRP) was carefully transferred to new 50-ml tubes containing 2 ml of acid citrate dextrose, further diluted to 50 ml total volume with room temperature Tyrodé's buffer, and spun at 700 g for 10 min at room temperature. Afterwards, the supernatant was discarded, and the platelet pellet was resuspended in 10 ml of room temperature Tyrodé's buffer. Platelets were treated with sialidase and analyzed using flow cytometry as described above.

Statistical analysis

All experiments were performed with a minimum of three independent replications. Data are presented as means ± SEM. For normally distributed data, unpaired two-tailed *t* test was used to determine the statistical significance between two groups. One-way ANOVA with post-hoc testing was used to determine

statistical significance between multiple groups. All statistical analyses were performed using GraphPad PRISM software (version 8.1.0).

Online supplemental material

Fig. S1 shows labeling of the vessel lumen with dextran right after injection (related to Fig. 1), repopulation of Kupffer cells (related to Fig. 2), absolute young and total platelet counts after Kupffer cell depletion (related to Fig. 2), galactose exposure on "old" platelets (related to Fig. 2), and accumulation of endogenously labeled platelets on Kupffer cells after sialidase injection (related to Fig. 3). Fig. S2 shows unaltered Kupffer cell phenotype (size and catching capability) of mice treated with arsenic in drinking water for 5 wk, which display a reduced number of fenestrations in liver sinusoids following this treatment (related to Fig. 3). Fig. S3 shows that there is no increase in platelet accumulation in the spleen or lung following sialidase treatment, that sialidase treatment leads to complete platelet removal also in splenectomized mice, and that bone marrow megakaryocytes do not phagocytose platelets. Fig. S4 shows unaltered Kupffer cell phenotype (size, total area, and catching capacity) in ST3Gal-IV^{Δ/Δ} mice (related to Fig. 3). Fig. S5 shows that 24 h after sialidase injection, the platelets that clustered on Kupffer cells are gone, that isolated Kupffer cells phagocytose platelets in vitro, that there is no difference in the accumulation of platelets on Kupffer cells following sialidase treatment in Mac1-deficient mice compared with wild-type mice, that AMR and MGL are expressed on mouse Kupffer cells, that *Asgr1*^{-/-} mice display unaltered platelet counts, and that human desialylated platelets bind human MGL. Video 1 shows that Kupffer cells are the intravascular, tissue-resident macrophage population of the liver. Video 2 shows that Kupffer cells form both transient and firm interactions with platelets under homeostatic conditions. Video 3 shows that, under naive conditions, platelets interact with and bind to Kupffer cells. Video 4 shows that Kupffer cells phagocytose platelets under naive conditions. Video 5 shows that ex vivo desialylated platelets rapidly adhere to Kupffer cells. Video 6 shows that Kupffer cell depletion prevents accumulation of ex vivo desialylated platelets. Video 7 shows that desialylated platelets rapidly adhere to Kupffer cells. Video 8 shows that platelets do not accumulate on splenic red pulp macrophages after sialidase injection. Video 9 shows that endogenously desialylated platelets from ST3Gal-IV^{Δ/Δ} mice bind to Kupffer cells. Video 10 shows that Kupffer cells phagocytose desialylated platelets. Video 11 shows that desialylated platelets accumulate inside Kupffer cells. Video 12 shows that desialylated platelets are transported to the phagolysosome in Kupffer cells. Video 13 shows that, in control mice, platelets rapidly accumulate on Kupffer cells after sialidase injection. Video 14 shows that, in ASF-pretreated mice, accumulation of platelets on Kupffer cells after sialidase injection is strongly reduced. Video 15 shows that, in AMR-deficient mice, platelets rapidly accumulate on Kupffer cells after sialidase injection. Video 16 shows that, in mice treated with an MGL-blocking antibody, platelets rapidly accumulate on Kupffer cells after sialidase injection. Video 17 shows that combining AMR deficiency with MGL blockade significantly reduced the amount of platelets accumulating on Kupffer cells after sialidase injection.

Acknowledgments

The authors would like to thank Thomas Graf (Centre for Genomic Regulation, Barcelona, Spain) for providing CD41-YFP mice, Trecia Nussbaumer for mouse breeding, Karen Poon at the Nicole Perkins Microbial Communities Core Labs for help with flow cytometry, and Ali Darbandi from the Microscopy and Imaging Facility for help with scanning EM. The authors would also like to thank Pina Colarusso and Andrew Chojnacki for assistance with image analysis.

This work was supported by the Live Cell Imaging Resource Laboratory. C. Deppermann and M. Peiseler are supported by Deutsche Forschungsgemeinschaft Research Fellowships DE 2654/1-1 and PE 2737/1-1, respectively. P. Kubes is supported by grants from the Canadian Institutes of Health Research, the Heart and Stroke Foundation of Canada, and the Canada Research Chairs program. J.D. Marth's support was provided by National Institutes of Health grants DK048247, L131474, and HL125352.

Author contributions: Conceptualization, C. Deppermann and P. Kubes; methodology, C. Deppermann, R.M. Kratoofil, M. Peiseler, A. Carestia, and C.N. Jenne; investigation, C. Deppermann, R.M. Kratoofil, M. Peiseler, B.A. David, J. Zindel, F.V.E.S. Castanheira, and F. van der Wal; writing (original draft), C. Deppermann and P. Kubes; writing (review and editing), C. Deppermann, J.D. Marth, and P. Kubes; funding acquisition, C. Deppermann and P. Kubes; resources, C.N. Jenne, J.D. Marth, and P. Kubes; and supervision, P. Kubes.

Disclosures: The authors declare no competing interests exist.

Submitted: 22 April 2019

Revised: 1 October 2019

Accepted: 17 December 2019

References

Ashwell, G., and A.G. Morell. 1974. The role of surface carbohydrates in the hepatic recognition and transport of circulating glycoproteins. *Adv. Enzymol. Relat. Areas Mol. Biol.* 41:99–128.

Aster, R.H. 1969. Studies of the fate of platelets in rats and man. *Blood*. 34: 117–128. <https://doi.org/10.1182/blood.V34.2.117.117>

Aster, R.H., and J.H. Jandl. 1964. Platelet sequestration in man. I. Methods. *J. Clin. Invest.* 43:843–855. <https://doi.org/10.1172/JCI104970>

Azimifar, S.B., N. Nagaraj, J. Cox, and M. Mann. 2014. Cell-type-resolved quantitative proteomics of murine liver. *Cell Metab.* 20:1076–1087. <https://doi.org/10.1016/j.cmet.2014.11.002>

Becker, G.A., M. Tuccelli, T. Kunicki, M.K. Chalos, and R.H. Aster. 1973. Studies of platelet concentrates stored at 22 C nad 4 C. *Transfusion*. 13: 61–68. <https://doi.org/10.1111/j.1537-2995.1973.tb05442.x>

Bender, M., S. Stritt, P. Nurdén, J.M.M. van Eeuwijk, B. Zieger, K. Kentouche, H. Schulze, H. Morbach, D. Stegner, K.G. Heinze, et al. 2014. Megakaryocyte-specific Profilin1-deficiency alters microtubule stability and causes a Wiskott-Aldrich syndrome-like platelet defect. *Nat. Commun.* 5:4746. <https://doi.org/10.1038/ncomms5746>

Bider, M.D., R. Cescato, P. Jenö, and M. Spiess. 1995. High-affinity ligand binding to subunit H1 of the asialoglycoprotein receptor in the absence of subunit H2. *Eur. J. Biochem.* 230:207–212. <https://doi.org/10.1111/j.1432-1033.1995.02071.x>

Bilzer, M., F. Roggel, and A.L. Gerbes. 2006. Role of Kupffer cells in host defense and liver disease. *Liver Int.* 26:1175–1186. <https://doi.org/10.1111/j.1478-3231.2006.01342.x>

Bouwens, L., M. Baekeland, R. De Zanger, and E. Wisse. 1986. Quantitation, tissue distribution and proliferation kinetics of Kupffer cells in

normal rat liver. *Hepatology*. 6:718–722. <https://doi.org/10.1002/hep.1840060430>

Braiterman, L.T., S.C. Chance, W.R. Porter, Y.C. Lee, R.R. Townsend, and A.L. Hubbard. 1989. The major subunit of the rat asialoglycoprotein receptor can function alone as a receptor. *J. Biol. Chem.* 264:1682–1688.

Cho, J., H. Kim, J. Song, J.W. Cheong, J.W. Shin, W.I. Yang, and H.O. Kim. 2018. Platelet storage induces accelerated desialylation of platelets and increases hepatic thrombopoietin production. *J. Transl. Med.* 16:199. <https://doi.org/10.1186/s12967-018-1576-6>

Tabula Muris Consortium. 2018. Single-cell transcriptomics of 20 mouse organs creates a Tabula Muris. *Nature*. 562:367–372. <https://doi.org/10.1038/s41586-018-0590-4>

Deniset, J.F., B.G. Surewaard, W.-Y. Lee, and P. Kubes. 2017. Splenic Ly6G^{high} mature and Ly6G^{int} immature neutrophils contribute to eradication of *S. pneumoniae*. *J. Exp. Med.* 214:1333–1350. <https://doi.org/10.1084/jem.20161621>

Deppermann, C., and P. Kubes. 2018. Start a fire, kill the bug: The role of platelets in inflammation and infection. *Innate Immun.* 24:335–348. <https://doi.org/10.1177/1753425918789255>

Devine, D.V., and K. Serrano. 2010. The platelet storage lesion. *Clin. Lab. Med.* 30:475–487. <https://doi.org/10.1016/j.cll.2010.02.002>

Ellies, L.G., D. Ditto, G.G. Levy, M. Wahrenbrock, D. Ginsburg, A. Varki, D.T. Le, and J.D. Marth. 2002. Sialyltransferase ST3Gal-IV operates as a dominant modifier of hemostasis by concealing asialoglycoprotein receptor ligands. *Proc. Natl. Acad. Sci. USA*. 99:10042–10047. <https://doi.org/10.1073/pnas.142005099>

Futterer, J., A. Dalby, G.C. Lowe, B. Johnson, M.A. Simpson, J. Motwani, M. Williams, S.P. Watson, and N.V. Morgan. UK GAPP Study Group. 2018. Mutation in *GNE* is associated with severe congenital thrombocytopenia. *Blood*. 132:1855–1858. <https://doi.org/10.1182/blood-2018-04-847798>

Grewal, P.K. 2010. The Ashwell-Morell receptor. *Methods Enzymol.* 479: 223–241.

Grewal, P.K., S. Uchiyama, D. Ditto, N. Varki, D.T. Le, V. Nizet, and J.D. Marth. 2008. The Ashwell receptor mitigates the lethal coagulopathy of sepsis. *Nat. Med.* 14:648–655. <https://doi.org/10.1038/nm1760>

Grewal, P.K., P.V. Aziz, S. Uchiyama, G.R. Rubio, R.D. Lardone, D. Le, N.M. Varki, V. Nizet, and J.D. Marth. 2013. Inducing host protection in pneumococcal sepsis by preactivation of the Ashwell-Morell receptor. *Proc. Natl. Acad. Sci. USA*. 110:20218–20223. <https://doi.org/10.1073/pnas.1313905110>

Grozovsky, R., A.J. Begonja, K. Liu, G. Visner, J.H. Hartwig, H. Falet, and K.M. Hoffmeister. 2015a. The Ashwell-Morell receptor regulates hepatic thrombopoietin production via JAK2-STAT3 signaling. *Nat. Med.* 21: 47–54. <https://doi.org/10.1038/nm.3770>

Grozovsky, R., S. Giannini, H. Falet, and K.M. Hoffmeister. 2015b. Regulating billions of blood platelets: glycans and beyond. *Blood*. 126:1877–1884. <https://doi.org/10.1182/blood-2015-01-569129>

Guidotti, L.G., D. Inverso, L. Sironi, P. Di Lucia, J. Fioravanti, L. Ganzer, A. Fiocchi, M. Vacca, R. Aiolfi, S. Sammiceli, et al. 2015. Immunosurveillance of the liver by intravascular effector CD8⁺ T cells. *Cell*. 161: 486–500. <https://doi.org/10.1016/j.cell.2015.03.005>

Gurney, A.L., K. Carver-Moore, F.J. de Sauvage, and M.W. Moore. 1994. Thrombocytopenia in c-mpl-deficient mice. *Science*. 265:1445–1447. <https://doi.org/10.1126/science.8073287>

Harrison, P., M.S.C. Robinson, I.J. Mackie, and S.J. Machin. 1997. Reticulated platelets. *Platelets*. 8:379–383. <https://doi.org/10.1080/09537109777050>

Helmy, K.Y., K.J. Katschke Jr., N.N. Gorgani, N.M. Kljavin, J.M. Elliott, L. Diehl, S.J. Scales, N. Ghilardi, and M. van Lookeren Campagne. 2006. CRIG: a macrophage complement receptor required for phagocytosis of circulating pathogens. *Cell*. 124:915–927. <https://doi.org/10.1016/j.cell.2005.12.039>

Hendriks, H.F.J., A. Brouwer, and D.L. Knook. 1990. Isolation, purification, and characterization of liver cell types. *Methods Enzymol.* 190:49–58.

Hoffmeister, K.M., and H. Falet. 2016. Platelet clearance by the hepatic Ashwell-Morell receptor: mechanisms and biological significance. *Thromb. Res.* 141(Suppl 2):S68–S72. [https://doi.org/10.1016/S0049-3848\(16\)30370-X](https://doi.org/10.1016/S0049-3848(16)30370-X)

Hoffmeister, K.M., T.W. Felbinger, H. Falet, C.V. Denis, W. Bergmeier, T.N. Mayadas, U.H. von Andrian, D.D. Wagner, T.P. Stossel, and J.H. Hartwig. 2003a. The clearance mechanism of chilled blood platelets. *Cell*. 112:87–97. [https://doi.org/10.1016/S0092-8674\(02\)01253-9](https://doi.org/10.1016/S0092-8674(02)01253-9)

Hoffmeister, K.M., E.C. Josefsson, N.A. Isaac, H. Clausen, J.H. Hartwig, and T.P. Stossel. 2003b. Glycosylation restores survival of chilled blood platelets. *Science*. 301:1531–1534. <https://doi.org/10.1126/science.1085322>

- Junt, T., H. Schulze, Z. Chen, S. Massberg, T. Goerge, A. Krueger, D.D. Wagner, T. Graf, J.E. Italiano Jr., R.A. Shivdasani, and U.H. von Andrian. 2007. Dynamic visualization of thrombopoiesis within bone marrow. *Science*. 317:1767–1770. <https://doi.org/10.1126/science.1146304>
- Kaushansky, K. 2005. The molecular mechanisms that control thrombopoiesis. *J. Clin. Invest.* 115:3339–3347. <https://doi.org/10.1172/JCI26674>
- Kaushansky, K., S. Lok, R.D. Holly, V.C. Broudy, N. Lin, M.C. Bailey, J.W. Forstrom, M.M. Buddle, P.J. Oort, F.S. Hagen, et al. 1994. Promotion of megakaryocyte progenitor expansion and differentiation by the c-Mpl ligand thrombopoietin. *Nature*. 369:568–571. <https://doi.org/10.1038/369568a0>
- Kauskot, A., T. Pascreau, F. Adam, A. Bruneel, C. Reperant, M.-D. Lourenco-Rodrigues, J.P. Rosa, R. Petermann, H. Maurey, C. Auditeau, et al. 2018. A mutation in the gene coding for the sialic acid transporter SLC35A1 is required for platelet life span but not proplatelet formation. *Haematologica*. 103:e613–e617. <https://doi.org/10.3324/haematol.2018.198028>
- Kienast, J., and G. Schmitz. 1990. Flow cytometric analysis of thiazole orange uptake by platelets: a diagnostic aid in the evaluation of thrombocytopenic disorders. *Blood*. 75:116–121. <https://doi.org/10.1182/blood.V75.1.116.116>
- Lee, W.-Y., T.J. Moriarty, C.H.Y. Wong, H. Zhou, R.M. Strieter, N. van Rooijen, G. Chaconas, and P. Kubas. 2010. An intravascular immune response to *Borrelia burgdorferi* involves Kupffer cells and iNKT cells. *Nat. Immunol.* 11:295–302. <https://doi.org/10.1038/ni.1855>
- Li, J., D.E. van der Wal, G. Zhu, M. Xu, I. Youghare, L. Ma, B. Vadasz, N. Carrim, R. Grozovsky, M. Ruan, et al. 2015. Desialylation is a mechanism of Fc-independent platelet clearance and a therapeutic target in immune thrombocytopenia. *Nat. Commun.* 6:7737. <https://doi.org/10.1038/ncomms8737>
- Li, R., K.M. Hoffmeister, and H. Falet. 2016. Glycans and the platelet life cycle. *Platelets*. 27:505–511. <https://doi.org/10.3109/09537104.2016.1171304>
- Li, Y., J. Fu, Y. Ling, T. Yago, J.M. McDaniel, J. Song, X. Bai, Y. Kondo, Y. Qin, C. Hoover, et al. 2017. Sialylation on O-glycans protects platelets from clearance by liver Kupffer cells. *Proc. Natl. Acad. Sci. USA*. 114: 8360–8365. <https://doi.org/10.1073/pnas.1707662114>
- Ng, W.C., S. Liang, M.D. Tate, T. Irimura, K. Denda-Nagai, A.G. Brooks, S.L. Londrigan, and P.C. Reading. 2014. The macrophage galactose-type lectin can function as an attachment and entry receptor for influenza virus. *J. Virol.* 88:1659–1672. <https://doi.org/10.1128/JVI.02014-13>
- Nishimura, S., M. Nagasaki, S. Kunishima, A. Sawaguchi, A. Sakata, H. Sakaguchi, T. Ohmori, I. Manabe, J.E. Italiano Jr., T. Ryu, et al. 2015. IL-1 α induces thrombopoiesis through megakaryocyte rupture in response to acute platelet needs. *J. Cell Biol.* 209:453–466. <https://doi.org/10.1083/jcb.201410052>
- Offermanns, S. 2006. Activation of platelet function through G protein-coupled receptors. *Circ. Res.* 99:1293–1304. <https://doi.org/10.1161/01.RES.0000251742.71301.16>
- Pang, Y.Y., J. Schwartz, M. Thoendel, L.W. Ackermann, A.R. Horswill, and W.M. Nauseef. 2010. agr-Dependent interactions of *Staphylococcus aureus* USA300 with human polymorphonuclear neutrophils. *J. Innate Immun.* 2:546–559. <https://doi.org/10.1159/000319855>
- Peng, J., P. Friese, E. Heilmann, J.N. George, S.A. Burstein, and G.L. Dale. 1994. Aged platelets have an impaired response to thrombin as quantitated by P-selectin expression. *Blood*. 83:161–166. <https://doi.org/10.1182/blood.V83.1.161.161>
- Pleines, I., M. Lebois, P. Gangatirkar, A.E. Au, R.M. Lane, K.J. Henley, M. Kauppi, J. Corbin, P. Cannon, J. Bernardini, et al. 2018. Intrinsic apoptosis circumvents the functional decline of circulating platelets but does not cause the storage lesion. *Blood*. 132:197–209. <https://doi.org/10.1182/blood-2017-11-816355>
- Quach, M.E., W. Chen, and R. Li. 2018. Mechanisms of platelet clearance and translation to improve platelet storage. *Blood*. 131:1512–1521. <https://doi.org/10.1182/blood-2017-08-743229>
- Rensen, P.C.N., L.A.J.M. Sliedregt, M. Ferns, E. Kieviet, S.M.W. van Rosenberg, S.H. van Leeuwen, T.J.C. van Berkel, and E.A.L. Biessen. 2001. Determination of the upper size limit for uptake and processing of ligands by the asialoglycoprotein receptor on hepatocytes in vitro and in vivo. *J. Biol. Chem.* 276:37577–37584. <https://doi.org/10.1074/jbc.M101786200>
- Revel-Vilk, S., E. Shai, E. Turro, N. Jahshan, E. Hi-Am, G. Spectre, H. Daum, Y. Kalish, K. Althaus, A. Greinacher, et al. 2018. GNE variants causing autosomal recessive macrothrombocytopenia without associated muscle wasting. *Blood*. 132:1851–1854. <https://doi.org/10.1182/blood-2018-04-845545>
- Rice, K.G., V.H. Thomas, and Y. Yang. 2003. Probing the binding specificity of C-type lectins in vivo. *Methods Enzymol.* 363:90–104. [https://doi.org/10.1016/S0076-6879\(03\)01045-0](https://doi.org/10.1016/S0076-6879(03)01045-0)
- Riswari, S.F., R.N. Tunjungputri, V. Kullaya, F.M. Garishah, G.S.R. Utari, N. Farhanah, G.J. Overheul, B. Alisjahbana, M.H. Gasem, R.T. Urbanus, et al. 2019. Desialylation of platelets induced by Von Willebrand Factor is a novel mechanism of platelet clearance in dengue. *PLoS Pathog.* 15: e1007500. <https://doi.org/10.1371/journal.ppat.1007500>
- Rumjantseva, V., P.K. Grewal, H.H. Wandall, E.C. Josefsson, A.L. Sørensen, G. Larson, J.D. Marth, J.H. Hartwig, and K.M. Hoffmeister. 2009. Dual roles for hepatic lectin receptors in the clearance of chilled platelets. *Nat. Med.* 15:1273–1280. <https://doi.org/10.1038/nm.2030>
- Schmitt, A., J. Guichard, J.M. Massé, N. Debili, and E.M. Cramer. 2001. Of mice and men: comparison of the ultrastructure of megakaryocytes and platelets. *Exp. Hematol.* 29:1295–1302. [https://doi.org/10.1016/S0301-472X\(01\)00733-0](https://doi.org/10.1016/S0301-472X(01)00733-0)
- Shao, L., Y. Wu, H. Zhou, P. Qin, H. Ni, J. Peng, and M. Hou. 2015. Successful treatment with oseltamivir phosphate in a patient with chronic immune thrombocytopenia positive for anti-GPIb/IX autoantibody. *Platelets*. 26:495–497. <https://doi.org/10.3109/09537104.2014.948838>
- Smedsrød, B., H. Pertoft, G. Eggertsen, and C. Sundström. 1985. Functional and morphological characterization of cultures of Kupffer cells and liver endothelial cells prepared by means of density separation in Percoll, and selective substrate adherence. *Cell Tissue Res.* 241:639–649. <https://doi.org/10.1007/BF00214586>
- Sørensen, A.L., V. Rumjantseva, S. Nayeb-Hashemi, H. Clausen, J.H. Hartwig, H.H. Wandall, and K.M. Hoffmeister. 2009. Role of sialic acid for platelet life span: exposure of β -galactose results in the rapid clearance of platelets from the circulation by asialoglycoprotein receptor-expressing liver macrophages and hepatocytes. *Blood*. 114:1645–1654. <https://doi.org/10.1182/blood-2009-01-199414>
- Straub, A.C., D.B. Stolz, M.A. Ross, A. Hernández-Zavala, N.V. Soucy, L.R. Klei, and A. Barchowsky. 2007. Arsenic stimulates sinusoidal endothelial cell capillarization and vessel remodeling in mouse liver. *Hepatology*. 45:205–212. <https://doi.org/10.1002/hep.21444>
- Stritt, S., S. Beck, I.C. Becker, T. Vögtle, M. Hakala, K.G. Heinze, X. Du, M. Bender, A. Braun, P. Lappalainen, and B. Nieswandt. 2017. Twinfilin 2a regulates platelet reactivity and turnover in mice. *Blood*. 130:1746–1756. <https://doi.org/10.1182/blood-2017-02-770768>
- Surewaard, B.G.J., and P. Kubas. 2017. Measurement of bacterial capture and phagosome maturation of Kupffer cells by intravital microscopy. *Methods*. 128:12–19. <https://doi.org/10.1016/j.jmeth.2017.05.004>
- Surewaard, B.G.J., R. Nijland, A.N. Spaan, J.A.W. Kruijtzter, C.J.C. de Haas, and J.A.G. van Strijp. 2012. Inactivation of staphylococcal phenol soluble modulins by serum lipoprotein particles. *PLoS Pathog.* 8:e1002606. <https://doi.org/10.1371/journal.ppat.1002606>
- Thanabalasuriar, A., B.G.J. Surewaard, M.E. Willson, A.S. Neupane, C.K. Stover, P. Warrener, G. Wilson, A.E. Keller, B.R. Sellman, A. DiGiandomenico, and P. Kubas. 2017. Bispecific antibody targets multiple *Pseudomonas aeruginosa* evasion mechanisms in the lung vasculature. *J. Clin. Invest.* 127:2249–2261. <https://doi.org/10.1172/JCI89652>
- Tozawa, R., S. Ishibashi, J. Osuga, K. Yamamoto, H. Yagyu, K. Ohashi, Y. Tamura, N. Yahagi, Y. Iizuka, H. Okazaki, et al. 2001. Asialoglycoprotein receptor deficiency in mice lacking the major receptor subunit. Its obligate requirement for the stable expression of oligomeric receptor. *J. Biol. Chem.* 276:12624–12628. <https://doi.org/10.1074/jbc.M011063200>
- Wandall, H.H., K.M. Hoffmeister, A.L. Sørensen, V. Rumjantseva, H. Clausen, J.H. Hartwig, and S.J. Slichter. 2008. Galactosylation does not prevent the rapid clearance of long-term, 4 ° C-stored platelets. *Blood*. 111: 3249–3256. <https://doi.org/10.1182/blood-2007-06-097295>
- Ward, S.E., J.M. O'Sullivan, C. Drakeford, S. Aguila, C.N. Jondle, J. Sharma, P.G. Fallon, T.M. Brophy, R.J.S. Preston, P. Smyth, et al. 2018. A novel role for the macrophage galactose-type lectin receptor in mediating von Willebrand factor clearance. *Blood*. 131:911–916. <https://doi.org/10.1182/blood-2017-06-787853>
- Warren, A., D.G. Le Couteur, R. Fraser, D.G. Bowen, G.W. McCaughan, and P. Bertolino. 2006. T lymphocytes interact with hepatocytes through fenestrations in murine liver sinusoidal endothelial cells. *Hepatology*. 44:1182–1190. <https://doi.org/10.1002/hep.21378>
- Wisse, E. 1970. An electron microscopic study of the fenestrated endothelial lining of rat liver sinusoids. *J. Ultrastruct. Res.* 31:125–150. [https://doi.org/10.1016/S0022-5320\(70\)90150-4](https://doi.org/10.1016/S0022-5320(70)90150-4)
- Wisse, E., F. Braet, D. Luo, R. De Zanger, D. Jans, E. Crabbé, and A. Vermoesen. 1996. Structure and function of sinusoidal lining cells in the liver. *Toxicol. Pathol.* 24:100–111. <https://doi.org/10.1177/019262339602400114>

- Wong, C.H.Y., C.N. Jenne, B. Petri, N.L. Chrobok, and P. Kubes. 2013. Nucleation of platelets with blood-borne pathogens on Kupffer cells precedes other innate immunity and contributes to bacterial clearance. *Nat. Immunol.* 14:785–792. <https://doi.org/10.1038/ni.2631>
- Xu, M., J. Li, M.A.D. Neves, G. Zhu, N. Carrim, R. Yu, S. Gupta, J. Marshall, O. Rotstein, J. Peng, et al. 2018. GPIIb is required for platelet-mediated hepatic thrombopoietin generation. *Blood.* 132:622–634. <https://doi.org/10.1182/blood-2017-12-820779>
- Yang, W.H., P.V. Aziz, D.M. Heithoff, M.J. Mahan, J.W. Smith, and J.D. Marth. 2015. An intrinsic mechanism of secreted protein aging and turnover. *Proc. Natl. Acad. Sci. USA.* 112:13657–13662. <https://doi.org/10.1073/pnas.1515464112>
- Yang, W.H., D.M. Heithoff, P.V. Aziz, B. Haslund-Gourley, J.S. Westman, S. Narisawa, A.B. Pinkerton, J.L. Millán, V. Nizet, M.J. Mahan, and J.D. Marth. 2018. Accelerated aging and clearance of host anti-inflammatory enzymes by discrete pathogens fuels sepsis. *Cell Host Microbe.* 24: 500–513.e5. <https://doi.org/10.1016/j.chom.2018.09.011>
- Zapotoczny, B., K. Szafranska, K. Owczarczyk, E. Kus, S. Chlopicki, and M. Szymonski. 2017. Atomic force microscopy reveals the dynamic morphology of fenestrations in live liver sinusoidal endothelial cells. *Sci. Rep.* 7:7994. <https://doi.org/10.1038/s41598-017-08555-0>
- Zeng, Z., B.G.J. Surewaard, C.H.Y. Wong, J.A. Geoghegan, C.N. Jenne, and P. Kubes. 2016. CRIG functions as a macrophage pattern recognition receptor to directly bind and capture blood-borne gram-positive bacteria. *Cell Host Microbe.* 20:99–106. <https://doi.org/10.1016/j.chom.2016.06.002>
- Zhang, J., F. Varas, M. Stadtfeld, S. Heck, N. Faust, and T. Graf. 2007. CD41-YFP mice allow in vivo labeling of megakaryocytic cells and reveal a subset of platelets hyperreactive to thrombin stimulation. *Exp. Hematol.* 35:490–499. <https://doi.org/10.1016/j.exphem.2006.11.011>

Supplemental material

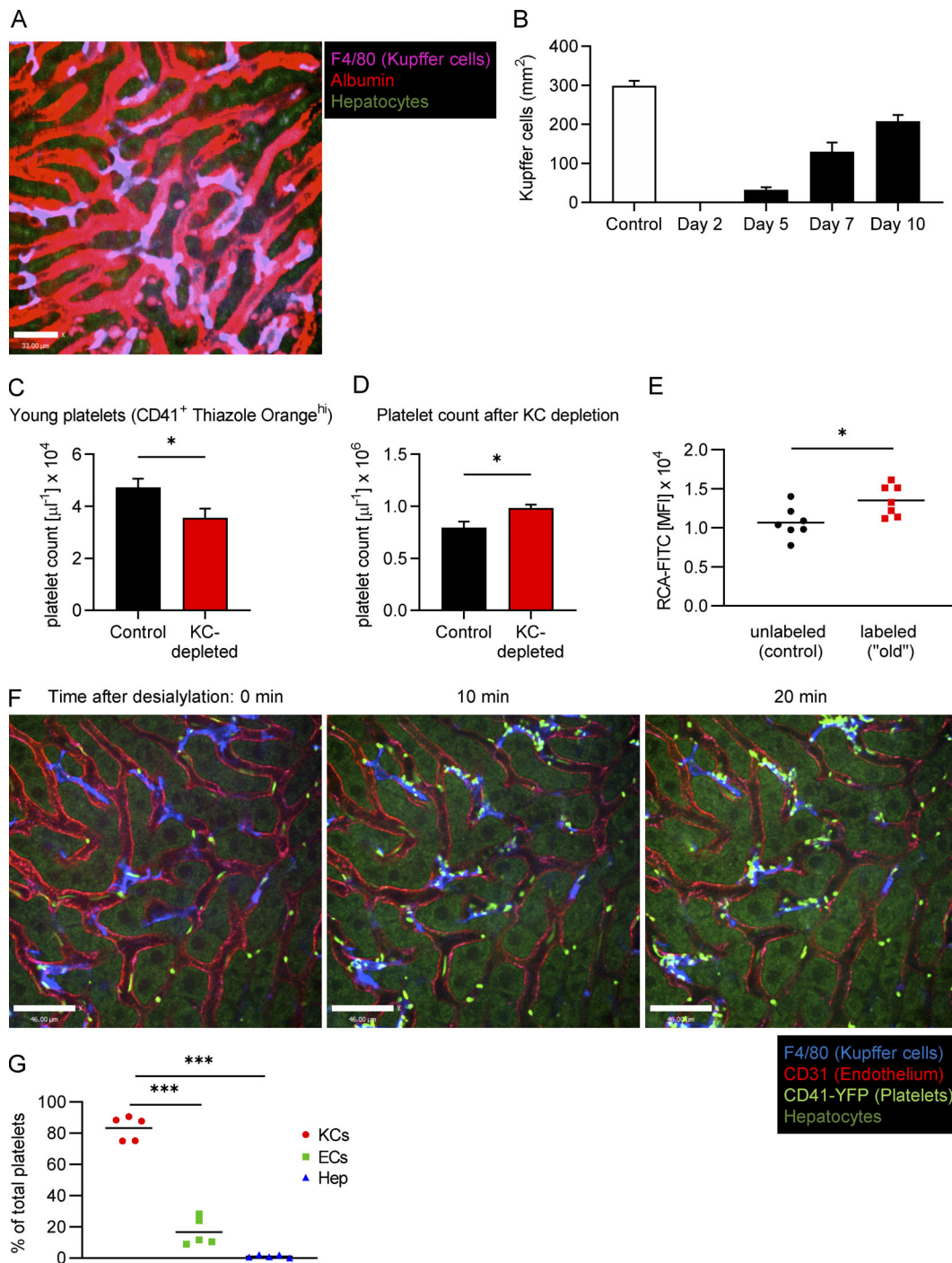


Figure S1. Following clodronate treatment, Kupffer cells start repopulating the liver from day 7, the number of young platelets decreases while the total platelet count increases and upon desialylation, and CD41-YFP platelets accumulate predominantly on Kupffer cells. (A) SD-IVM of the mouse liver right after injection of fluorescently labeled albumin. Kupffer cells were stained using fluorescently labeled anti-F4/80 antibody. Scale bar is 33 μm . **(B)** Mice were treated with a single dose of i.v. clodronate liposomes to deplete Kupffer cells. Kupffer cell repopulation was quantified as the F4/80-positive area over time. Data represent means \pm SEM ($n \geq 5$ mice per group). **(C)** Quantification of the CD41⁺ Thiazole Orange^{hi} young platelet population in the blood from control mice and mice on day 5 after Kupffer cell (KC) depletion. Data represent means \pm SEM ($n = 5$ mice per group). **(D)** Total platelet count was analyzed using flow cytometry of blood from control mice and mice on day 5 after Kupffer cell depletion. Data represent means \pm SEM ($n = 5$ mice per group). **(E)** Galactose exposure as measured by RCA-FITC binding to control and "old" platelets on day 3 after in vivo labeling. Data represent means \pm SEM ($n = 7$ mice per group). **(F)** SD-IVM of the liver of CD41-YFP^{ki/+} mice treated with 50 mU sialidase. Representative still images obtained at the indicated time points. Kupffer cells and endothelial cells were stained using fluorescently labeled anti-F4/80 and anti-CD31 antibody, respectively. Scale bars are 46 μm . **(G)** Colocalization of platelets with Kupffer cells, endothelial cells (ECs), and hepatocytes (Hep) was quantified at the 20-min time point after sialidase treatment using Imaris software. Data represent means \pm SEM ($n = 5$ mice per group). Unpaired two-tailed *t* test (C–E) and one-way ANOVA with post-hoc testing (G) were used to determine statistical significance. *, $P < 0.05$; ***, $P < 0.001$. Results from all experiments shown are representative of at least three independent experiments.

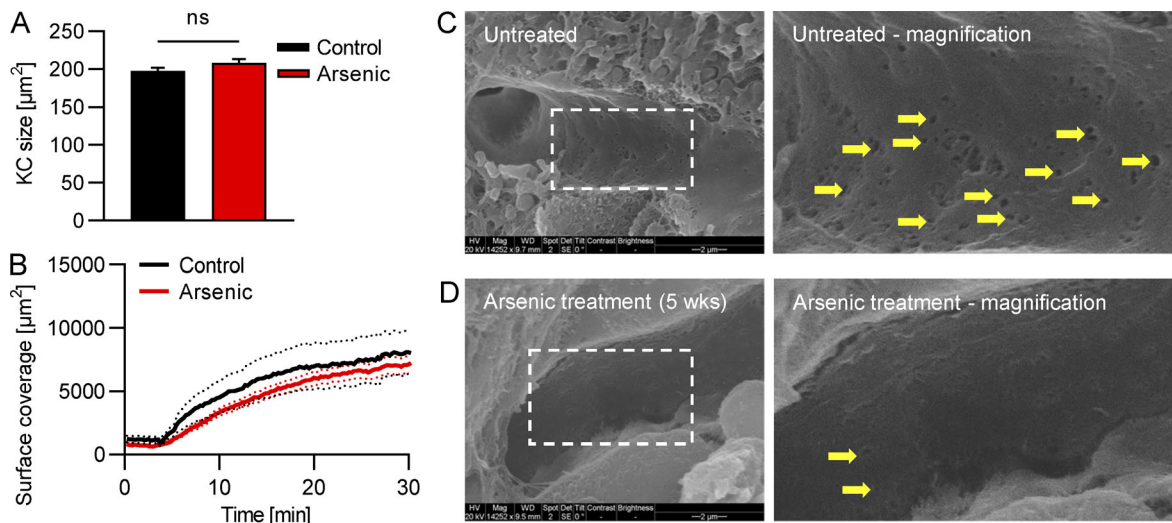


Figure S2. **Unaltered Kupffer cell size and recruitment of desialylated platelets but reduced fenestrations in mice after arsenic treatment.** Mice were treated with arsenic in their drinking water for 5 wk. **(A)** Quantification of the Kupffer cell size from SD-IVM images. Data represent means \pm SEM ($n = 5$ mice). **(B)** Quantification of the accumulation of platelets in the liver after sialidase treatment. $n = 5$ mice. **(C and D)** Representative scanning EM images of the liver sinusoids show less fenestrations (arrows) after arsenic treatment. Scale bars are 2 μm . Unpaired two-tailed t test (A) was used to determine statistical significance. ns, not significant. Results from all experiments shown are representative of at least three independent experiments.

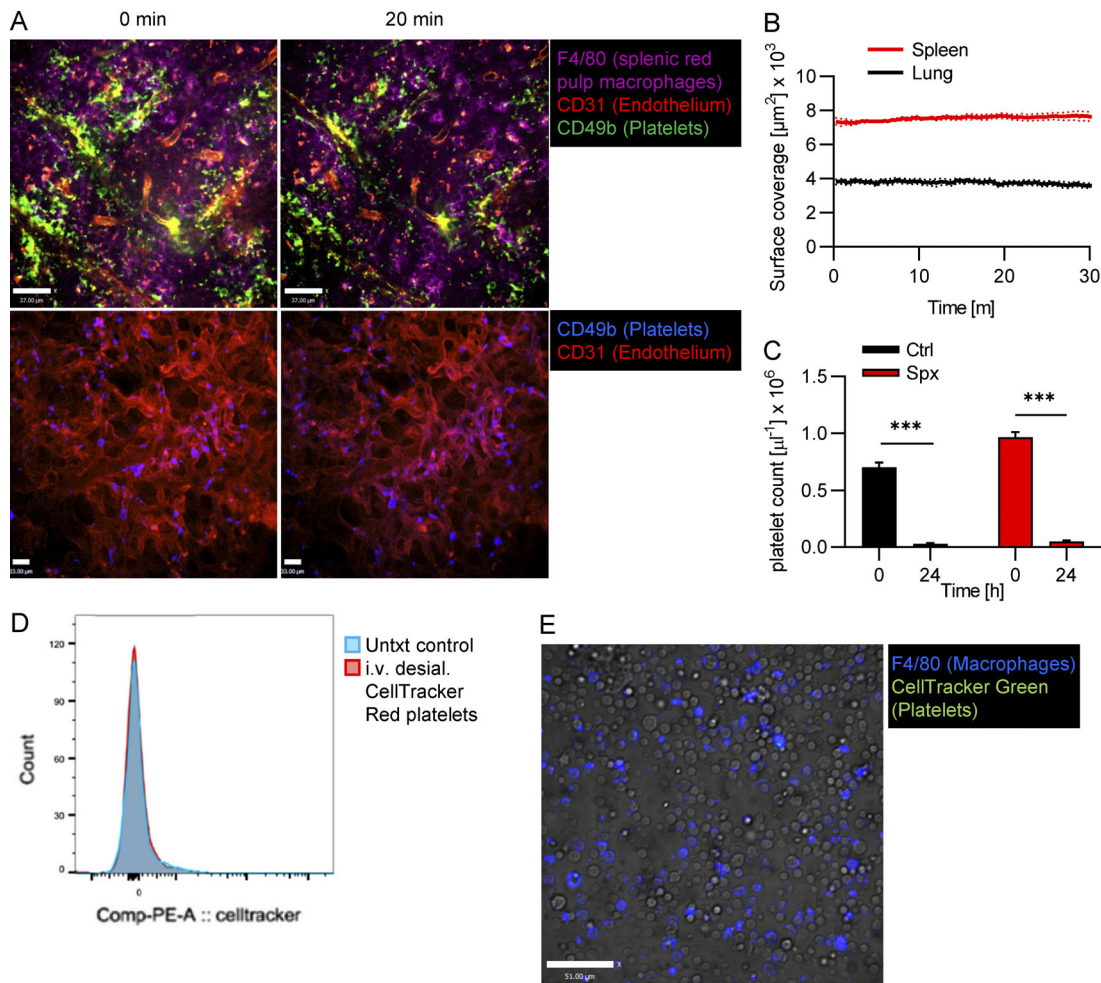


Figure S3. **No accumulation of desialylated platelets in the spleen, lung, or bone marrow.** (A) Mice were i.v. injected with 50 mU sialidase, and platelet recruitment in the spleen (upper panel) and lung (lower panel) was investigated using SD-IVM. Representative images at the indicated time points after desialylation. Splenic red pulp macrophages, endothelial cells, and platelets were stained using anti-F4/80, anti-CD31, and anti-CD49b antibodies, respectively. Scale bars are 37 μm (top row) and 33 μm (bottom row). (B) Quantification of the accumulation of platelets in the spleen and lung upon desialylation. $n = 3$ mice. (C) Splenectomized (Spx) mice were treated with sialidase, and the platelet count was measured before and 24 h after treatment. $n = 5$ mice. (D and E) Mice were i.v. injected with ex vivo desialylated CellTracker-labeled platelets. 1 h later, the bone marrow was flushed out and analyzed. Flow cytometry shows no CellTracker signal in viable $\text{CD45}^+ \text{CD11b}^+ \text{F4/80}^+$ bone marrow macrophages (D). Fluorescence microscopy shows no CellTracker signal in F4/80^+ bone marrow macrophages. Scale bar is 51 μm (E). Unpaired two-tailed t test (C) was used to determine statistical significance. ***, $P < 0.001$. Results from all experiments shown are representative of at least three independent experiments.

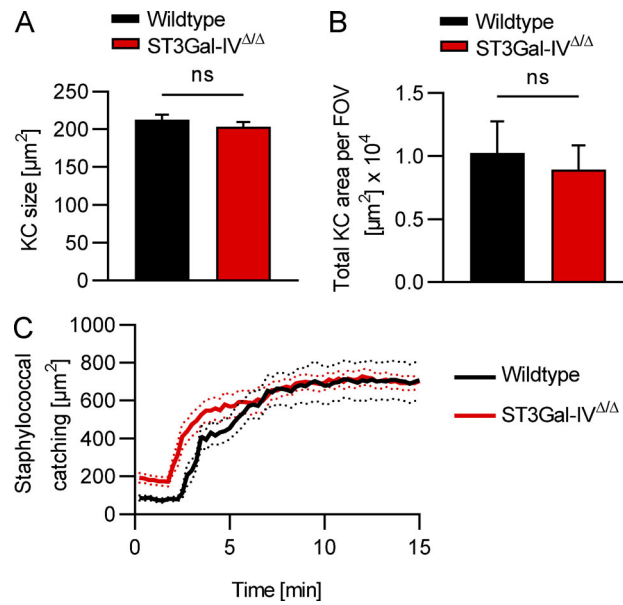


Figure S4. **Unaltered Kupffer cell size, number, and function in ST3Gal-IV^{Δ/Δ} mice.** (A and B) Kupffer cell (KC) size (A) and total Kupffer cell area per field of view (FOV; B) of wild-type and ST3Gal-IV^{Δ/Δ} mice were quantified from SD-IVM images. (C) Kupffer cell function in wild-type and ST3Gal-IV^{Δ/Δ} mice was assessed by studying staphylococcal catching after i.v. injection of 5×10^7 CFU of *S. aureus* MW2. Unpaired two-tailed *t* test (A and B) was used to determine statistical significance. ns, not significant. Results from all experiments shown are representative of at least three independent experiments.

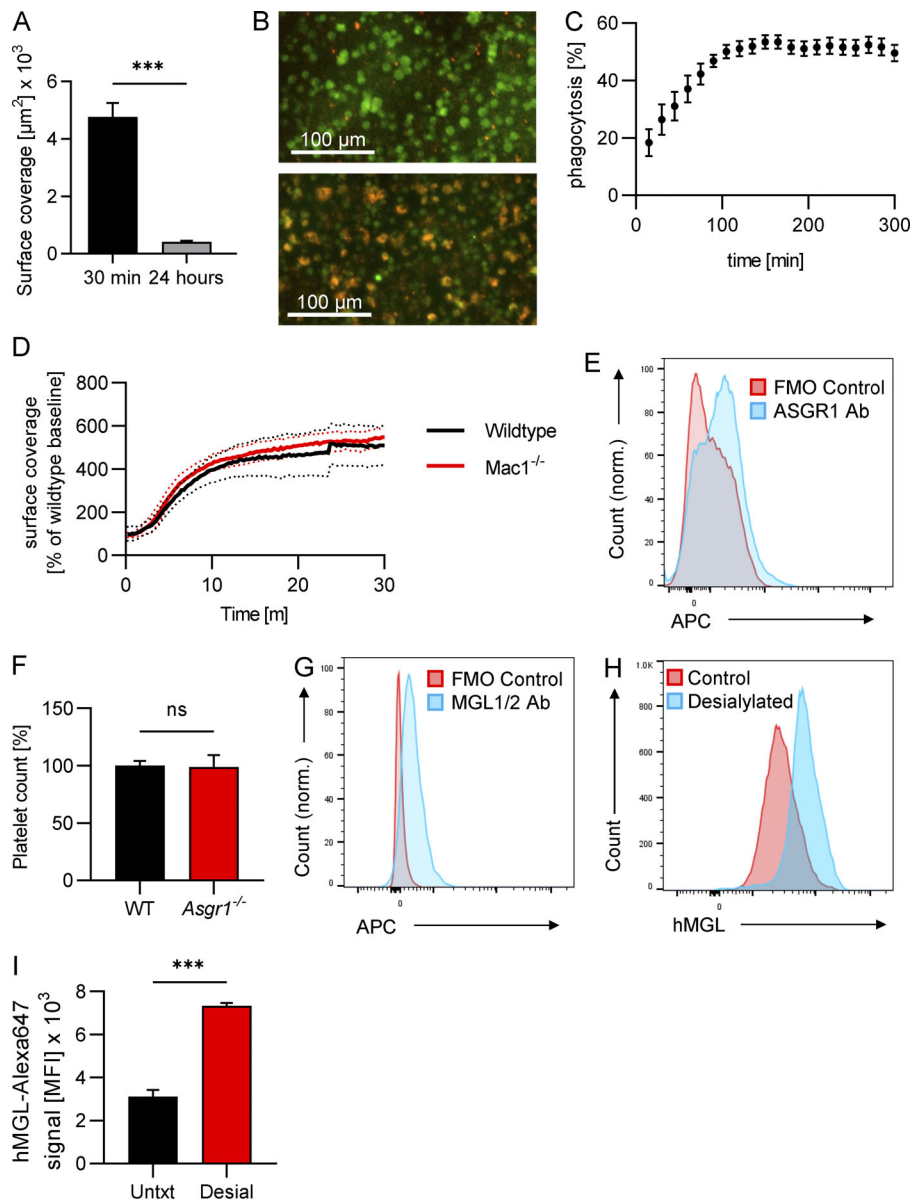


Figure S5. Desialylated platelets are phagocytosed by Kupffer cells in vitro, Mac1 is dispensable for the clearance of desialylated platelets, Kupffer cells express Asgr1 and MGL1/2, but Asgr1-deficiency alone has no effect on platelet count. (A) Mice were treated with 50 mU sialidase i.v., and the amount of platelet accumulation in the liver at 30 min and 24 h after treatment was quantified as the CD49b-positive area from images obtained using SD-IVM. Data represent means \pm SEM ($n \geq 3$ mice per group). (B) Kupffer cells were incubated with platelets in vitro, and phagocytosis was observed using an IncuCyte incubation microscope. Kupffer cells and platelets were labeled using F4/80 antibodies and CellTracker Red dye, respectively. Representative images showing Kupffer cell platelet co-culture at 0 h (upper panel) and at 5 h (lower panel). (C) Quantification of phagocytosis (Kupffer cells with red platelet signal inside) over time. (D) Wild-type and *Mac1*^{-/-} mice were i.v. injected with 50 mU sialidase, and platelet accumulation in the liver was quantified from SD-IVM videos. $n = 5$ mice per group. (E) Kupffer cells were isolated from mouse liver, and ASGR1 expression was analyzed using flow cytometry. Representative flow plot showing ASGR1 signal versus fluorescence minus one (FMO). (F) Platelet count in blood from wild-type and *Asgr1*^{-/-} mice was quantified using flow cytometry. Data represent means \pm SEM ($n = 5$ mice per group). (G) Kupffer cells were isolated from mouse liver and MGL expression analyzed using flow cytometry. Representative flow plot showing MGL signal versus fluorescence minus one (FMO). (H) Washed human platelets and desialylated washed human platelets were incubated with fluorescently labeled recombinant human MGL (hMGL), and binding was quantified using flow cytometry. Representative flow plot. (I) Quantification of the binding of hMGL to control and desialylated human platelets from healthy human volunteers. Data represent means \pm SEM ($n = 3$). Unpaired two-tailed *t* test (A, F, and I) was used to determine statistical significance. ***, $P < 0.001$; ns, not significant. Results from all experiments shown are representative of at least three independent experiments.

Video 1. **Kupffer cells are the intravascular, tissue-resident macrophage population of the liver.** 3D reconstruction of a z-stack obtained using SD-IVM of the mouse liver. Kupffer cells (purple), endothelial cells (blue), and the vascular lumen (red) were stained using an anti-F4/80 antibody, anti-CD31 antibody, and albumin, respectively. Frame rate is 10 frames per second (fps).

Video 2. **Kupffer cells form both transient and firm interactions with platelets under homeostatic conditions.** Imaris image analysis software was used to quantify interactions between Kupffer cells (turquoise, generated using the surface function) and platelets (small gray spheres, generated using the spot function). Representative video showing one long-term interaction (yellow sphere). Frame rate is 30 fps.

Video 3. **Under naive conditions, platelets interact with and bind to Kupffer cells.** SD-IVM of the mouse liver of CD41-YFP^{ki/+} mice. Kupffer cells (blue) were stained using an anti-F4/80 antibody. Endogenous platelets (bright green) are labeled with YFP. Hepatocytes are shown in dark green (autofluorescence). Frame rate is 20 fps.

Video 4. **Kupffer cells phagocytose platelets under naive conditions.** 3D reconstruction of a Kupffer cell from CD41-YFP^{ki/+} mice. Kupffer cells (blue) were stained using an anti-F4/80 antibody. Endogenous platelets (green) are labeled with YFP. Frame rate is 10 fps.

Video 5. **Ex vivo desialylated platelets rapidly adhere to Kupffer cells.** Time-lapse SD-IVM of the mouse liver after i.v. injection of ex vivo desialylated platelets (CellTracker Green) and control platelets (CellTracker Red). Kupffer cells (blue) were stained using an anti-F4/80 antibody. Hepatocytes are shown in dark green (autofluorescence). Frame rate is 20 fps.

Video 6. **Kupffer cell depletion prevents accumulation of ex vivo desialylated platelets.** Time-lapse SD-IVM video of the liver of mice pretreated with clodronate liposomes to deplete Kupffer cells after i.v. injection of ex vivo desialylated platelets (CellTracker Green) and control platelets (CellTracker Red). Kupffer cells (blue) were stained using an anti-F4/80 antibody. Hepatocytes are shown in dark green (autofluorescence). Frame rate is 20 fps.

Video 7. **Desialylated platelets rapidly adhere to Kupffer cells.** Time-lapse SD-IVM video of the mouse liver after i.v. injection of 50 mU sialidase. Kupffer cells (magenta), endothelial cells (blue), and platelets (white) were stained using anti-F4/80, anti-CD31, and anti-CD49b antibodies, respectively. Frame rate is 20 fps.

Video 8. **Platelets do not accumulate on splenic red pulp macrophages after sialidase injection.** Time-lapse SD-IVM video of the spleen of control mice after i.v. injection of 50 mU sialidase. Red pulp macrophages (purple), endothelial cells (red), and platelets (green) were labeled using anti-F4/80, anti-CD31, and anti-CD49b antibodies, respectively. Frame rate is 20 fps.

Video 9. **Endogenously desialylated platelets from ST3Gal-IV^{Δ/Δ} mice bind to Kupffer cells.** Time-lapse SD-IVM video of the liver of ST3Gal-IV^{Δ/Δ} mice. Kupffer cells (blue) were stained using an anti-F4/80 antibody. Endogenous platelets (red) were labeled using an anti-CD49b antibody. Hepatocytes are shown in dark green (autofluorescence). Frame rate is 20 fps.

Video 10. **Kupffer cells phagocytose desialylated platelets.** SD-IVM of the mouse liver after i.v. injection of ex vivo desialylated platelets (CellTracker Red). Kupffer cells (blue) were stained using an anti-F4/80 antibody. Hepatocytes are shown in dark green (autofluorescence). Frame rate is 30 fps.

Video 11. **Desialylated platelets accumulate inside Kupffer cells.** 3D reconstruction of a z-stack obtained using SD-IVM after i.v. injection of ex vivo desialylated platelets. Kupffer cells (blue) were stained using an anti-F4/80 antibody. Ex vivo desialylated platelets (red) were labeled using CellTracker Red dye. Frame rate is 10 fps.

Video 12. **Desialylated platelets are transported to the phagolysosome in Kupffer cells.** 3D reconstruction of a z-stack obtained using SD-IVM after i.v. injection of ex vivo desialylated platelets loaded with the pH indicator pHrodo. Kupffer cells (white) were stained using an anti-F4/80 antibody. Ex vivo desialylated platelets (blue) were labeled using Alexa Fluor 647 and loaded with pHrodo (red). Frame rate is 10 fps.

Video 13. **In control mice, platelets rapidly accumulate on Kupffer cells after sialidase injection.** Time-lapse SD-IVM video of the liver of control mice after i.v. injection of 50 mU sialidase. Kupffer cells (blue) were stained using an anti-F4/80 antibody. Endogenous platelets (red) were labeled using an anti-CD49b antibody. Frame rate is 20 fps.

Video 14. **In ASF-pretreated mice, accumulation of platelets on Kupffer cells after sialidase injection is strongly reduced.** Time-lapse SD-IVM video of the liver of mice pretreated with ASF after i.v. injection of 50 mU sialidase. Kupffer cells (blue) were stained using an anti-F4/80 antibody. Endogenous platelets (red) were labeled using an anti-CD49b antibody. Frame rate is 20 fps.

Video 15. **In AMR-deficient mice, platelets rapidly accumulate on Kupffer cells after sialidase injection.** Time-lapse SD-IVM video of the liver of *Asgr1*^{-/-} mice after i.v. injection of 50 mU sialidase. Kupffer cells (blue) were stained using an anti-F4/80 antibody. Endogenous platelets (red) were labeled using an anti-CD49b antibody. Frame rate is 20 fps.

Video 16. **In mice treated with an MGL-blocking antibody, platelets rapidly accumulate on Kupffer cells after sialidase injection.** Time-lapse SD-IVM video of the liver of wild-type mice treated with MGL1/2 blocking antibody and injected i.v. with 50 mU sialidase. Kupffer cells (blue) were stained using an anti-F4/80 antibody. Endogenous platelets (red) were labeled using an anti-CD49b antibody. Frame rate is 20 fps.

Video 17. **Combining AMR deficiency with MGL blockade significantly reduced the amount of platelets accumulating on Kupffer cells after sialidase injection.** Time-lapse SD-IVM video of the liver of *Asgr1*^{-/-} mice treated with MGL1/2 blocking antibody and injected i.v. with 50 mU sialidase. Kupffer cells (blue) were stained using an anti-F4/80 antibody. Endogenous platelets (red) were labeled using an anti-CD49b antibody. Frame rate is 20 fps.